OUKA
Osaka University Knowledge Archive

Title	Anomalous Behaviour of the Cyclotron Resonance in Bismuth
Author(s)	中原, 純一郎
Citation	大阪大学, 1971, 博士論文
Version Type	VoR
URL	https://hdl.handle.net/11094/1690
rights	
Note	

Osaka University Knowledge Archive : OUKA

https://ir.library.osaka-u.ac.jp/

Osaka University

ANOMALOUS BEHAVIOUR OF THE CYCLOTRON RESONANCE IN BISMUTH

by

Jun'ichiro NAKAHARA

ACKNOWLEDGEMENT

I am deeply grateful to my advisor, Professor H. Kawamura, for his constant encouragement, suggestions, and enlightening discussions, without which this thesis would not have been possible.

I wish to thank Drs. Y. Sawada and S. Takano for their many helpful discussions and for patiently answering to my many questions.

I wish to thank Professor Y. Uemura and Mr. T. Akahane of Tokyo University for their very stimulating discussions.

The technical assistance of Drs. S. Nagata and K. Murase is greatly appreciated.

The co-operation of fellow graduate students O. Shimomura, N. Hoshi, K. Toyoda and S. Ohta is also appreciated.

I wish to thank Mr. I. Asai at the low temperature laboratory of Osaka University for supplying liquid He.

I wish to thank Dr. D. Snider for reading the manuscript.

Finally, I wish to thank Miss A. Nishijima for her help in typing.

SYNOPSIS

Cyclotron resonance in bismuth has been carefully investigated using microwaves of 50 GHz at liq.He temperature in the Azbel'-Kaner configuration by the field derivative method. Anomalous behaviour of the Azbel'-Kaner type cyclotron resonance is observed. The reflection peak is extremely weak at the fundamental but strong at the second harmonic, and the line shape of the harmonic is quite complicated for the hole cyclotron resonances which occur in a weakly nonlocal condition, especially in the case when the hole cyclotron frequency is less than the electron-hole hybrid frequency. This is explaied if a longitudinal magnetoplasma excitation and a transverse excitation (Bernstein mode and $\omega = n\omega_c$) are coupled with the electromagnetic waves in a magnetoplasma. Further, the strength of the nth harmonic cyclotron resonance decreases rapidly as the order increases for electrons even though $\omega\tau$ was large. For a field lower than the electron-hole hybrid resonance, electromagnetic waves do not penetrate into the plasma and the coupling is extremely weak. In this case the coupled mode corresponds to the so-called high frequency waves. The sbsorption is due to this coupled mode. These phenomena are quite different from those for metals which are explained by the extremely nonlocal theory.

Contents

I. INTRODUCTION

Electromagnetic waves are usually reflected from the surface of high conductivity materials when the frequency ω is lower than the plasma frequency ω_p. However, since Galt and Buchsbaum[1] showed that in certain compensated conductor (such as bismuth) magnetohydrodynamic or Alfven waves could also be propagated as in gas plasmas, many experimental and theoretical investigations[2)-13)] have been performed on magnetoplasmas in bismuth. Smith and his coworkers investigated the some properties of the local magnetoplasmas under a classical skin effect condition.[3] They observed a dielectric anomaly, hybrid resonance, tilted orbit cyclotron resonance, and Alfven waves.[3)9)-12)] Such a wave is a disturbance which is harmonic or nearly harmonic in both time and space, and which is able to propagate deep into the plasmas under classical skin effect condition. Further, quantum effects have been investigated by the detailed analysis of Alfven waves.[10)-12)] The typical phase velocity of these waves is very low. In fact they are lower than the Fermi velocities of carriers. The nonlocal effects for spherical and ellipsoidal Fermi surfaces were analyzed by cyclotron damping of Alfven waves for Faraday configuration.[13)] It was found that the effects for both cases were different.

The phenomena related to the anomalous skin effect[14)] such as Azbel'-Kaner cyclotron resonance,[15)] surface skipping orbit,[16)-19)] and size effect of Gantmakher[20)] appear in the extremely nonlocal limit $qv_F/\omega_c \gg 1$, which is equivalent to $R \gg \delta$. Hebel has discussed a slightly anomalous skin effect when the r.f. electric

fields of the microwaves (70 GHz) are parallel to the static magnetic field ($E_{rf}//B_o$, ordinary configuration).[8] He found that the cyclotron resonance due to the dipole transitions arising from the transverse excitation occured for the fundamental in this case. However, in the extraordinary configuration ($E_{rf}\perp B_o$) the Alfven waves can propagate for $\omega_{ce}\omega_{ch} \gg \omega^2$, and cyclotron resonances occur for electrons under the condition $qv_{Fe}/\omega_{ce} \geq 1$. Furthermore the hole cyclotron resonances in bismuth occur in a weakly nonlocal condition, especially in the case that the hole cyclotron frequency is less than the electron-hole hybrid frequency $\sqrt{\omega_{ce}\omega_{ch}}$. In this case the longitudinal component of the dielectric constant should play an important role.

In this thesis the waves under a local, an extremely nonlocal, and a weakly nonlocal conditions are comprehensively treated. Under a weakly nonlocal condition we shall present both the experimental and the calculation for the anomalous line shape of the hole cyclotron resonances. Especially in the extraordinary configuration, our data indicate that the reflection peak near the second harmonic is the strongest of the peaks associated with either the fundamental or other harmonics. In addition, the line shape of the reflection peak may be quite complicated. This behaviour is quite different from those for metals which occur under extremely nonlocal limit with large values of $\omega\tau$, in which case the line shapes depend upon the structure of the Fermi surface as was explained by Chambers[21] and experimentally shown by Moore.[22]

II. ELEMENTS OF THE THEORY OF THE MAGNETOPLASMAS IN SOLIDS

a. Absorption and Surface Impedance

The observable electromagnetic properties of a metal are described by the surface impedance Z(0) defined as

$$Z = R + iX = \frac{4\pi}{c}\frac{E_t}{H_t} = \frac{4\pi}{c}\frac{E_t(0)}{E_t'(0)}\ , \qquad (1)$$

where E_t and H_t are the tangential components of $\vec{E}$ and $\vec{H}$ evaluated at the surface of a metal (y-z plane). The real part R of Z determines the power absorption by the metal. The rate of energy loss per unit area normal to the metal surface (x=0) is given by the time average of the real part of the Poynting vector $\vec{S}$ which magnitude is given by

$$|\vec{S}| = \frac{c}{4\pi}\,|\mathrm{Re}(\vec{H}\times\vec{E})| = \left(\frac{c}{4\pi}\right)^2 R H_t^2\ , \qquad (2)$$

when the fields are evaluated at x=+0.

Now consider Maxwell's equations

$$\mathrm{div}\ \vec{B}(\vec{r},t) = 0, \qquad (3a)$$

$$\mathrm{div}\ \vec{D}(\vec{r},t) = 0, \qquad (3b)$$

$$\mathrm{rot}\ \vec{E}(\vec{r},t) = -\frac{1}{c}\frac{\partial}{\partial t}\vec{B}(\vec{r},t), \qquad (3c)$$

$$\mathrm{rot}\ \vec{H}(\vec{r},t) = \frac{1}{c}\left\{\frac{\partial}{\partial t}\vec{D}(\vec{r},t) + 4\pi\vec{J}(\vec{r},t)\right\}. \qquad (3d)$$

From the divergence equations it follows that in a plane wave of the form $\vec{E} = \vec{E}\exp(i\vec{q}\cdot\vec{r} - i\omega t)$, the B-field of the wave is transverse, but the E-field is not always so.

In the fourth Maxwell's equation the conduction current J is assumed to be linearly related to electric field E. In general, the relation between J and E is nonlocal even when linear. We

shall assume that J is proportional to E through a tensor conductivity which is a function of the frequency ω.

We assume the specular reflection of the carriers at the surface. If we consider the remaining half of space ($x<0$) filled with another piece of the same metal, the carriers in each half will have the same history as if the reflection were specular. We must only provide the proper electric field at x=0. The gradient of this artificial field will have a cusp at x=0, because the field is damped in both $\pm x$ directions;

$$\frac{\partial}{\partial x} E_t)_{x=+0} = - \frac{\partial}{\partial x} E_t)_{x=-0} . \qquad (4)$$

Considering this condition, we express each term as a fourier transformation and find

$$-q^2 E_q + \frac{\omega^2}{c^2} \varepsilon_1 E_q = - \frac{4\pi i \omega}{c^2} J_q + \sqrt{\frac{2}{\pi}} \frac{\partial}{\partial x} E)_{x=+0} . \qquad (5)$$

The transport equation gives us the relation $J_q = \sigma_q E_q$.
We obtain the electric field in the metal

$$E(x) = \frac{1}{\pi} \frac{\partial E}{\partial x})_{+0} \int_{-\infty}^{+\infty} dq \frac{e^{iqx}}{-q^2 + \frac{\omega^2}{c^2} \varepsilon_1 + \frac{4\pi i \omega}{c^2} \sigma_q} , \qquad (6)$$

The surface impedance Z is found from Eqs. (1) and (6)

$$Z = \frac{8 i \omega}{c^2} \int_0^{\infty} dq \frac{1}{-q^2 + \frac{\omega^2}{c^2} \varepsilon_\ell + \frac{4\pi i \omega}{c^2} \sigma_q} , \qquad (7)$$

where $\sigma_q = \sigma_{zz}(q)$ for ordinary mode, or

$$\sigma_q = \sigma_{yy}(q) + \frac{\sigma_{xy}^2(q)}{\frac{4\pi}{i\omega} \varepsilon_1 + \sigma_{xx}(q)} \quad \text{for extraordinary mode.}$$

If q_o satisfies the dispersion relation, the denominator $q^2 - \frac{\omega^2}{c^2}\varepsilon_1 - \frac{4\pi i\omega}{c^2}\sigma_q$ is equal to zero for $q=q_o$, and the fields inside the metal are proportional to $\exp(iq_o x)$.

b. Conductivity Tensor for Spatial Dispersion

The current density J is given by

$$\vec{J} = \frac{2e}{h^3}\int \vec{v} f(\vec{r},\vec{v},t)\,d^3p \ , \qquad (8)$$

where $f(\vec{r},\vec{v},t)$ is the distribution function in phase space for carriers of the charge e, velocity $\vec{v}$, and position $\vec{r}$. When the electromagnetic field is absent, the distribution function reduces to the thermal equilibrium Fermi-Dirac function $f_0(\vec{v},E_F^0)$, (E_F^0 being the Fermi energy),and does not depend explicitly upon the static magnetic field $\vec{H}$. When a self-consistent electromagnetic field is present, the distribution function is determined from Boltzmann's equation: ($\phi = \omega_c t$)

$$\frac{\partial}{\partial t} f + \vec{v}\cdot \mathrm{grad} f + \omega_c \frac{\partial f}{\partial \phi} + \frac{f - f_0}{\tau} = e\vec{E}\cdot\vec{v}\frac{\partial f_0}{\partial \varepsilon} \ . \qquad (9)$$

By a method due to Chambers[23] the distribution function is given by

$$f = f_0 + \frac{\partial f_0}{\partial \varepsilon}\int_{-\infty}^{\phi} d\phi' \frac{e\vec{E}(\phi')\vec{v}(\phi')}{\omega_c} \exp\left\{\frac{1-i\omega\tau}{\omega_c\tau}(\phi'-\phi) + \frac{i}{\omega_c}\int_{\phi}^{\phi'} \vec{q}\,\vec{v}(\phi'')\,d\phi''\right\}. \qquad (10)$$

For an arbitrary Fermi surface, the elements of the magneto-conductivity have the form (see Appendix A)

$$\sigma_{\alpha\beta}(\vec{q},\omega,\omega_c) = \frac{2e^2}{h^3}\int_0^{\infty} d\varepsilon \frac{m_c}{\omega_c}\frac{\partial f_0}{\partial \varepsilon_F}\int_{-\infty}^{+\infty} dp_z \int_0^{2\pi} d\phi\, v_\alpha(\varepsilon_F, p_z, \phi)$$

$$\times \int_{-\infty}^{+\Phi} d\phi' v_\beta(\varepsilon_F, p_z, \phi') \exp\left\{\frac{1-i\omega\tau}{\omega_c\tau}(\phi'-\phi) + \frac{i}{\omega_c}\int_{\phi}^{\phi'} \vec{q}\,\vec{v}(\phi'')\,d\phi''\right\}. \qquad (11)$$

For simplicity, we shall assume that the energy surfaces are

spherical. The properties of the magnetoplasmas are not changed by this simplification in the Voigt configuration.[13]

We arrive at the following expression of the conductivity tensor

$$\overleftrightarrow{\sigma} = \frac{3\sigma_0}{2} \sum_{n=-\infty}^{+\infty} \int_0^{\pi} \left[\begin{pmatrix} \frac{n}{X} \\ i\frac{\partial}{\partial X} \\ \cos\theta \end{pmatrix} J_n(X\sin\theta) \right] \times \left[\begin{pmatrix} \frac{n}{X} \\ -i\frac{\partial}{\partial X} \\ \cos\theta \end{pmatrix} J_n(X\sin\theta) \right] \times \frac{\sin\theta \, d\theta}{1 + i(n\omega_c - \omega + q_z v_F \cos\theta)} , \qquad (12)$$

where $X = q_x v_F/\omega_c$ and $\sigma_0 = ne^2\tau/m$.

The quantum mechanical discussions for the conductivity have been given by Mattis and Dresselhauss,[24] by Zyryanov,[25] by Zyryanov and Kalashinikov,[26] and by Quinn and Rodriguez.[27] When the carriers are degenerate and the Landau level spacings are much less than the Fermi energy ($E_F \gg kT, \hbar\omega_c$), the components of the conductivity tensor reduce to the expressions given above. The numerator for each n is proportional to the oscillator strength for single particle excitations in the field of wave number q.

For the propagation in a transverse magnetic field (q is perpendicular to H), the components of the conductivity for each kind of carriers are given by (q//x, H//z)[27][28]

$$\sigma_{xx} = \frac{3\sigma_0}{X^2} \sum_{n=-\infty}^{+\infty} \frac{n^2 \beta_n(X)}{1 + i(n\omega_c - \omega)\tau} , \qquad (13a)$$

$$\sigma_{yy} = 3\sigma_0 \sum_{n=-\infty}^{+\infty} \frac{s_n(X)}{1 + i(n\omega_c - \omega)\tau} , \qquad (13b)$$

$$\sigma_{xy} = -\sigma_{yx} = \frac{3\sigma_0}{2X} \sum_{n=-\infty}^{+\infty} \frac{in g_n'(X)}{1 + i(n\omega_c - \omega)\tau} , \qquad (13c)$$

and

$$\sigma_{zz} = 3\sigma_0 \sum_{n=-\infty}^{+\infty} \frac{r_n(X)}{1 + i(n\omega_c - \omega)\tau} , \qquad (13d)$$

where

$$g_n(X) = \sum_{m=0}^{\infty} \frac{(-1)^m X^{2m+2n}}{m!(m+2n)!(2m+2n+1)} , \qquad (14a)$$

$$s_n(X) = (2 + \frac{n^2}{X^2}) g_n(X) - 3 \sum_{m=0}^{\infty} \frac{(-1)^m 2(m+n+1) X^{2m+2n}}{m!(m+2n)!(2m+2n+1)(2m+2n+3)} , \qquad (14b)$$

$$r_n(X) = \sum_{m=0}^{\infty} \frac{(-1)^m X^{2m+2n}}{m!(m+2n)!(2m+2n+1)(2m+2n+3)} . \qquad (14c)$$

Using the conductivity formalism we shall discuss in the following sections the properties of the magneto plasmas: the local, the extremely nonlocal, and the weakly nonlocal plasmas.

c. Alfven Waves (Local) ----- High Field Approximation (X=0)

When the wave frequency ω is much smaller than the cyclotron frequencies ω_{cj} (j: electrons or holes), the motion of charge carriers about the lines of force of the magnetic field is adiabatic for the closed orbit in the absence of the waves. This means that the carriers are tied to the lines of force and must move with them. It follows that the amplitude of oscillation induced by the electric field $\vec{E}$ of the waves in a direction at right angles to $\vec{H}$ and $\vec{E}$ is the same for all carriers and is independent of their mass. It also follows, therefore, that the electric current in the Hall direction is zero in the above approximation if the plasma is compensated, because then equal densities of positive and negative charge oscillate in phase with equal amplitudes. But there is mass motion in the Hall direction and it is the kinetic energy of this mass motion which determines the dispersion of the waves.[29)]

In the above approximation (which is equivalent to $qv_F/\omega_c \ll 1$; i.e. $R \ll \delta$), we may put X = 0 in Eqs. (13) and (14). Then from the Eq. (6) the field E in the metal is given by the following equation;

$$E(x) = E_o \exp(iq_o x) + E_\delta \exp(iq_o x), \qquad (15)$$

where $q_o^2 = \omega^2 \varepsilon_1 / c^2 + 4\pi i \omega / c^2 \sigma_{q=0}$ (this is a dispersion relation). But for finite $\omega\tau$ we can calculate the field from from Eq. (6), and the absorption from Eq. (7), because the integral function has no pole on real axis of q and E'(0) is not zero. The dispersion relations for Voigt configuration

are given by

$$\left(\frac{c}{\omega} q_e\right)^2 = \varepsilon_\ell + \frac{\varepsilon_\ell (\omega_{ce}^2 - \omega^2)(\omega_{ch}^2 - \omega^2) + (\omega_{pe}^2 + \omega_{ph}^2)^2}{(\omega_{ce}^2 - \omega^2)(\omega_{ch}^2 - \omega^2)\varepsilon_\ell + \omega_{pe}^2(\omega_{ch}^2 - \omega^2) + \omega_{ph}^2(\omega_{ce}^2 - \omega^2)}, \quad (16)$$

$$= \varepsilon_\ell - \frac{\omega_{pe}^2}{\omega^2} - \frac{\omega_{ph}^2}{\omega^2}. \quad (17)$$

Especially for the extraordinary mode, the dispersion relation under the conditions of our experiment ($\omega_p^2 \gg \omega^2$) is

$$\left(\frac{c}{\omega} q_e\right)^2 = \varepsilon_\ell + \frac{\omega_{pe}^2 + \omega_{ph}^2}{|\omega_{ce}\omega_{ch}| - \omega^2}, \quad (18)$$

$$\cong 4\pi c^2 n(m_e + m_h)/H^2 \quad \text{for } \omega_{ce}\omega_{ch} \gg \omega^2. \quad (19)$$

This mode is called the Alfven waves under local conditions and has the properties of the longitudinal ($\omega_{ce}\omega_{ch} = \omega^2$) and transverse ($\omega_{ce}\omega_{ch} \gg \omega^2$) waves. The Alfven speed ω/k for high fields is independent of frequency, but depends on the mass density $n(m_e + m_h)$ and is therefore different for different direction in an anisotropic solid and varies for the change in carrier density and Fermi energy due to the quantum effects in high magnetic fields.[12]

d. Azbel'-Kaner Cyclotron Resonance ---- Low Field Approximation ($qR \gg 1$)

In the limit $v_F q/\omega_c \gg 1$ ($R \gg \delta$), it is found from the asymptotic formula of Eqs. (14) that

$$\sigma_{yy}(q) \cong \sigma_{zz}(q) \cong \frac{3\pi}{4} \frac{ne^2}{m} \frac{1}{qv_F} \coth\left(\frac{1 - i\omega\tau}{\omega_c\tau}\pi\right), \qquad (20)$$

which shows periodic oscillations provided that $\omega\tau, \omega_c\tau \gg 1$. In the same limit the surface impedance in the extremely anomalous region with specular reflection is

$$Z(H) = Z(0) \cdot \tanh^{1/3}\left(\frac{1 - i\omega\tau}{\omega_c\tau}\pi\right). \qquad (21)$$

These expressions are valid for $qv_F/\omega_c > n$ (n: order of the cyclotron harmonics); when n exceeds qv_F/ω_c, $g_n(X)$ and $s_n(X)$ become small. If we take the asymptotic formula for $g_n(X)$ and etc., we commit an error of the form of the final term in the following equation

$$\sum_{n=-\infty}^{+\infty} \frac{g_n(X)}{1 + i(n\omega_c - \omega)\tau} = \frac{1}{X} \frac{\pi}{\omega_c\tau} \coth\left(\frac{1 - i\omega\tau}{\omega_c\tau}\pi\right) - \frac{1}{X} \sum_{n=-\infty}^{+\infty} \frac{\int_{zx}^{\infty} J_{2n}(X)dX}{1 + i(n\omega_c - \omega)\tau}. \qquad (22)$$

The last term is nearly equal to the first term for $X < n$, but for $X > n$ this term is of the order of $X^{-3/2}$. [28]

At the resonance $\omega/\omega_c = n$, both the real and imaginary parts of the surface impedance are minimum at the case of a quadratic dispersion law and of an infinite $\omega\tau$.[15] The attenuation due to the collisions makes the impedance converges to the zero magnetic field value.

e. Nonlocal Magnetoplasma Excitations

The longitudinal excitation, which corresponds to the collective mode of a plasma, occurs when the condition:

$$\varepsilon_{xx} = \varepsilon_1 - \frac{4\pi}{i\omega} \sum_j \sigma^j_{xx} = 0, \quad (q//x, B//z) \qquad (23)$$

is fulfilled.

The transverse excitation, which corresponds to the single particle excitation, is given by the following equations:

$$\varepsilon_{yy} = \varepsilon_1 - \frac{4\pi}{i\omega} \sum_j \sigma^j_{yy} = \infty, \qquad (24)$$

or

$$\varepsilon_{zz} = \varepsilon_1 - \frac{4\pi}{i\omega} \sum_j \sigma^j_{zz} = \infty, \qquad (25)$$

From these relations we can determine the dispersion relations for those excitations if the frequency and wave number dependent dielectric functions shown in Eqs. (13) are employed.

The transverse excitation occurs at $\omega = n\omega_c$. For the longitudinal excitation we leave the lowest order term for the longitudinal component of the effective dielectric functions in a long wavelength approximation ($X < 1$). We will consider the case when the electron cyclotron frequency is much larger than the hole cyclotron frequency. In this case the electrons contribute to the dielectric function with a term varying smoothly as a function of the electron cyclotron frequency, so that effects of electrons can be included in ε_0. The longitudinal excitation near the lower harmonics of hole cyclotron frequency can be obtained from the following equation in the approximation including the terms up to X^2,

$$\varepsilon_{xx} \cong \varepsilon_0 + \frac{\omega_{p1}^2}{\omega_c^2 - \omega^2} + \frac{\omega_{p2}^2}{\omega_c^2 - \omega^2} = 0, \quad (26)$$

where the oscillator strengths ω_{p1}^2 and ω_{p2}^2 are given by

$$\omega_{p1}^2 = \omega_p^2(1 - X^2/5), \text{ and } \omega_{p2}^2 = \omega_p^2 X^2/5. \quad (27)$$

The solutions of Eq. (26) for $\omega_p^2/\varepsilon_0 \gg \omega_c^2$ are given by

$$\omega_+^2 = \omega_p^2/\varepsilon_0 + \omega_c^2 + 3q^2 v_F^2/5, \quad (28)$$

and

$$\omega_-^2 = (2\omega_c)^2 - 3q^2 v_F^2/5. \quad (29)$$

The higher mode ω_+ is well-known magnetoplasma excitation which exists even for q=0 (hybrid plasma mode or plasma shifted cyclotron resonance). The lower mode ω_-, which can exist only for finite q, corresponds to the Bernstein mode in a nondegenerate plasma.[30-31] This excitation ω_- appears only in the vicinity of the second harmonic in a long wavelength approximation up to the order of X^2. It is interesting to note that for this mode the group velocity and the phase velocity are in opposite directions. Further the longitudinal excitations appear only in the vicinity of the second harmonic cyclotron frequency and the hybrid plasma mode, because $\omega_{p1}^2 \gg \omega_c^2$, and $\omega_{p1} \gg \omega_{p2}$. If the next higher order terms up to X^4 are included, the longitudinal excitations near the third harmonic appear. In general, the longitudinal excitations near the nth harmonic appear at X^{2n-2}, because the effective plasma frequency ω_{pn} is smaller than ω_c. $(n \geq 2)$

f. Coupling of the Electromagnetic Waves with Nonlocal Magnetoplasma Mode

Electromagnetic waves couple with the transverse and the longitudinal excitations when the static magnetic field and wave vector are perpendicular to each other. One of these coupled mode is polarized along the magnetic field, and this mode is pure transverse because there is no magnetoresistance (ordinary mode). The other mode is polarized in the plane normal to the magnetic field, and this mode changes from the longitudinal to the transverse waves (extraordinary mode).

The dispersion relations of these coupled modes are obtained from the Maxwell's equations and q-dependent dielectric functions. The results are given by

$$\left(\frac{c}{\omega}q\right)^2 = \varepsilon_{zz}, \tag{30}$$

for the ordinary mode, and

$$\left(\frac{c}{\omega}q\right)^2 = \varepsilon_{yy} + \frac{\varepsilon_{xy}^2}{\varepsilon_{xx}}, \tag{31}$$

for the extraordinary mode.

Let us now consider the spectra of the electromagnetic excitations in solid state plasma with an equal number of electrons and holes. Wave propagation was observed in the vicinity of Azbel'-Kaner cyclotron resonance, which is called high frequency wave, for potassium.[32] In contrast to both the helicon and Alfven waves, its phase velocity($v = \omega/k$) scarecely depends on the velocity of the electromagnetic waves but does depend on the Fermi velocity of carriers. In this sense the plasma waves which are called high frequency waves are like sound waves whereas the

the helicon and Alfven waves are electromagnetic waves. The dispersion relation is given by

$$\left(\frac{c}{\omega} q\right)^2 = 1 - \frac{\omega_p^2}{\omega^2}\left[1 + \frac{X^2}{5(1 - \omega_c^2/\omega^2)} + \text{-----}\right], \quad (32)$$

near the fundamental cyclotron resonance for $X \ll 1$ on the ordinary mode. But the extraordinary mode is very complicated because this mode couples with longitudinal excitation and transverse excitation shown in Eqs. (23) and (24), respectively. We have solved Eq. (31) for fictitous semimetal having spherical electron and hole energy surfaces and being $m_e \ll m_h$. The conductivity functions were expanded up to X^{20} and the roots were found graphically as shown in Fig. 1. The model chosen here to simulate bismuth with magnetic field parallel to the bisectrix axis has the following features:

1. electron mass $m_e = 0.02 m_o$, hole mass $m_h = 0.21 m_o$,
2. carrier densities for electrons and holes = $2.9 \times 10^{17} \text{cm}^{-3}$,
3. Fermi velocities $v_{Fe} = 9 \cdot 10^7 \text{cm/sec}$, $v_{Fh} = 3 \cdot 10^7 \text{cm/sec}$.

In Fig. 2 the result of the calculation in the neighbourhood of the second harmonic of the hole cyclotron resonance are shown as solid lines. The microwave frequency is assumed to be 52.5 GHz, and the effect of carrier scattering is neglected. In Fig. 2 the longitudinal excitation, transverse excitation, and local Alfven waves for the Voigt configuration (extraordinary mode) are also shown as broken lines. The solid line indicates the coupling of the Alfven waves with longitudinal or transverse excitations. Strong microwave reflection would be expected to occur between points A and B, since in this region the real wave number does not

exist as a consequence of the assumption of an infinite relaxation time. The gap between A and B is nearly equal to $0.3q^2v_{Fh}^2m_hc/e/\omega$.

For the weakly nonlocal magnetoplasma ($X \ll 1$), such a strong reflection peak is not expected to occur for either the fundamental or for the third and higher harmonics, and the anomaly in the dispersion relation near the fundamental is negligibly small because the plasma frequency ω_{pl} is much larger than the cyclotron frequency. The longitudinal excitation appears only in the vicinity of the second harmonic as discussed in Sec.II e.

As the transverse excitation $\varepsilon_{yy}^{-1} = 0$ occurs at each cyclotron harmonic, the dispersion relation for the transverse waves is

$$\omega = n\omega_c\left(1 - \frac{\omega_p^2}{c^2}R^2\,\frac{1}{X^3}\,\frac{3}{4}\right) \qquad (33)$$

for a short wavelength approximation. In the long wavelength approximation the transverse escitations appear if the higher order terms are included. However, all the transverse excitations disappear at the lowest order expansion (X^2), since the longitudinal electric field creates a space charge which shields out the transverse resonances in the lowest order.[33)]

g. The Surface Quantum State

The surface impedance was calculated by a perturbative technique first used by R. E. Prange and T. W. Nee[16-17] for magnetic surface levels and by H. D. Drew and U. Strom[34] for corrections to the line-shape theory[21] due to retardation effect. For unperturbed fields the exponential functions were used to approximate the anomalous skin effect fields. While we refer the serious reader to the detailed theoretical discussion by Prange and Nee[16-17], we sketch here the surface quantum states to provide the necessary background for the present experiments. In the weak magnetic fields (0 to a few ten Oe), the microwave fields penetrate to a characteristic skin depth on the order of 10^{-5}cm, but the cyclotron radius R is typically on the order of 10^{-2}cm. Only those for which the electrons are moving essentially parallel to the surface, will make an important contribution to the surface currents out of the entire spectrum of possible colliding orbits. We restrict our attention to electrons moving along the surface with velocity v_y approximately equal to v_F, the Fermi velocity. Moreover, we may take v_y to be essentially constant throughout each cycle of the skipping motion and consequently the electrons see the potential

$$\begin{aligned} v(X) &= ev_F Hx \qquad (x \gtrsim 0), \\ &= \infty \qquad\quad (x < 0). \end{aligned} \tag{34}$$

We are therefore concerned with a particle confined in a triangular potential well. The electrons go arround between the surface and the classical turning point of its periodic motion. From the Bohr- Sommerfeld quantization rule we obtain

$$\oint P_x dx = 2\int_0^{x_n} P_F\sqrt{\frac{2(x_n-x)}{R}}\,dx = (n-\tfrac{1}{4})h, \qquad (35)$$

where P has been expressed in terms of the Fermi momentum P_F and appropriate geometrical factors. R represents the radius of the skipping trajectory. The phase factor of ¼ is chosen appropriately for the case of a single turning point of the motion. The possible energy states $\mathcal{E}_n$ (as measured from the Fermi energy E_F) are described in terms of quantum mechanically allowed values of the maximum depth of penetration x_n as

$$\mathcal{E}_n = ev_F H x_n. \qquad (36)$$

Evaluating the integral and solving for x_n we obtain

$$x_n = \left(\frac{3}{4\sqrt{2}}(n-\tfrac{1}{4})\frac{hR^{1/2}}{P_F}\right)^{2/3} = \left|\frac{3}{4}\sqrt{\pi}(n-\tfrac{1}{4})\right|^{2/3}\left(\frac{h}{eHK}\right)^{1/3}, \qquad (37)$$

Where R is the cyclotron radius, K the radius of curvature of the Fermi surface in K-space. Consequently, we obtain the energy-level scheme for the surface states

$$\mathcal{E}_n = \left|\frac{3}{4}\pi(n-\tfrac{1}{4})\right|^{2/3}(e^2h)^{1/3}H^{2/3}v_F K^{-1/3}. \qquad (38)$$

Since we have made use of the Bohr-Sommerfeld rule in our derivation, the energy level scheme in Eq.(38) differs from the expression derived by strict argument by about 1% for the lowest-lying level.[18]

Prange, Nee and Koch derived the surface impedance due to the surface state making use of a perturbation method.[16-17] Their result is given by

$$\frac{dZ}{dH} = -\frac{ie^2}{\hbar(2\pi)^2}\,[Z(0)]^2\,\frac{d}{dH}\int dk_z\, v_y \sum_{n,m}\frac{\alpha_{mn}(k_z,H,\delta)}{\omega-\omega_{mn}+i\Gamma_{mn}}$$

III. PROPERTIES OF BISMUTH

Bismuth belongs to the fifth group of the periodic table and have a rhombohedral crystal structure. This structure can be derived from a face centered cubic structure by applying an internal displacement of atoms and a shear distortion both along the body diagonal directions. The Brillouin zone for this structure and and several important symmetry points are shown in the following. figure

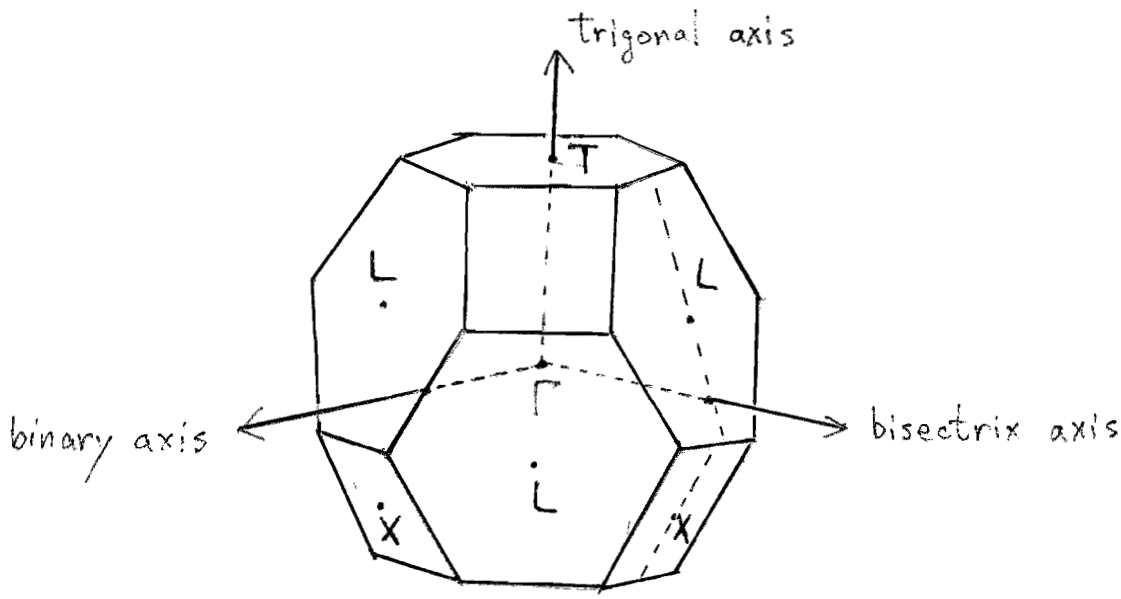

Bismuth is a typical semimetal which has carrier concentrations of 2.9×10^{17} cm^{-3} for electrons and holes, and is a useful material to investigate the magnetoplasmas in solids because of a long relaxation time. The Fermi surfaces of free carriers in bismuth have been extensively studied by various methods. Probable locations of Fermi surfaces in the Brillouin are L at the centres of the six pseudohexagonal faces for the six half-ellipsoids for electrons and T, centres of the perfect hexagonal faces for the two

half-ellipsoids for holes. Shoenberg's work on the de Haas-van Alphen effect has shown that one of the ellipsoids for electrons can be descrived in the crystallographic axis system by

$$2m_o E^* = \vec{P}\cdot\overleftrightarrow{\alpha}_e\cdot\vec{P}, \tag{40}$$

where

$$\overleftrightarrow{\alpha}_e^{-1} = \overleftrightarrow{m}_e = \begin{pmatrix} m_{xx} & 0 & 0 \\ 0 & m_{yy} & m_{yz} \\ 0 & m_{yz} & m_{zz} \end{pmatrix} \tag{41}$$

is the effective mass tensor, E^* the energy, and P is the quasi-momentum. The other two ellipsoids are generated by rotating the ellipsoid through $\pm 120^\circ$ about the trigonal axis.

The hole band is made up of an ellipsoid of revolution about the trigonal axis, it is

$$2m_o(E - E_b) = \vec{P}\cdot\overleftrightarrow{\alpha}_h\cdot\vec{P}, \tag{42}$$

where

$$\overleftrightarrow{\alpha}_h^{-1} = \overleftrightarrow{m}_h = \begin{pmatrix} M_z & 0 & 0 \\ 0 & M_x & 0 \\ 0 & 0 & M_z \end{pmatrix} \tag{43}$$

is the effective mass, E_b the band overlap energy, and $E - E_b$ the hole energy.

In the table 1, the paramerters which have been obtained up to now as well as those in the present experiments are listed. Appendix B

IV. EXPERIMENTAL ASPECTS

a. Preparation of Sample

Comercially available bismuth metals of nominal purity of 99.9999% were zone refined about thirty times by multizones in a high purity carbon boat and a vacuum higher than 8×10^{-7} torrs. The ingot was crystalized with a long furnace having a sharp temperature gradient at the front part, and smoother gradient at middle and rear part, travelling in the same direction as the refining furnaces with the speed of 3 cm/hour. The carbon boat had been baked at 600°C for a few days. The crystal was anealed for one day at 200°C, then the temperature was decreased at a rate of 20°C/hour.

The crystal ingot is cleaved in the trigonal plane. When the surface is chemically polished by 30% nitric acid solution, several etch lines parallel to the binary axis appear. By this method, the crystalographic axes were determined. The crystal was cut in the form of parallel plate or wedge shape with its thickness 0.3-3 mm. The block was planed using a spark planer, and the surfaces were made flat very carefully. Further, iregularities on the surface was removed by chemical polishing (30% nitric acid) and by electropolishing.[36)]

b. Measuring Technique and Experimental Apparatus

The experimental was performed with standard microwave technique at frequencies near 50 GHz. Magnetic field derivative of surface impedance as a function of magnetic fields was observed by detecting the change in Q or in the resonant frequency of a TE 113 cylindrical cavity of which the bismuth sample is mounted on a choke joint in a horizontal plate forming the small part of one end wall. In order to observe cyclotron resonances we took care of that the sample and the cavity were in contact. But the sumple was mounted to the joint with silicon grease softly not to distort the crystal. The cavity and the sample were in the exchange gas so as not to be impressed in liquid helium because the disturbance due to the change of the liquid helium surface in the wave guide was supressed. The microwave power from a stabilized klystron was branched at a magic tee, and a part of the power was transmitted to the cavity while the other part was fed into a matched load. The reflected power from the cavity was detected at the fourth arm of the magic tee by a crystal detector. The output voltage of the crystal was fed into a linear amplifier, a narrow band amplifier and then a phase sensitive detector, and recorded as a function of magnetic field. The modulation magnetic field is parallel to the d.c. magnetic field. The d.c. magnetic field was measured by the Hall probe calibrated by the nuclear magnetic resonances of protons and lithiums and by the electron spin resonance of DPPH from 500 gauss to 25 kG. The measurement of the magnetic fields from zero gauss to 400 gauss was done with the Hall probe and

exciting current. The field value due to those two methods differ less than 1.5%. Hall voltage and current producing the magnetic field are linearly proportional to magnetic fields.

The cavity has two orthogonal and degenerate modes in which the microwave currents across the wall are perpendicular to each other. In the cavity one mode is excited about ten times stronger than the other, as was checked by the electron spin resonance signal of DPPH.

The experimental response is the field derivative of absorption or reflected power from the sample which is nearly proportional to the field derivative of the real part of surface impedance Z for $c/4\pi \gg Z$. The temperature of the specimen was kept during the experiment at 1.6—1.7°K. A temperature increase to 4.2°K resulted in a broadening of the peaks and a reduction in their amplitude, corresponding to a reduction of the relaxation time by a factor 4/3, differing between different groups of carriers and different sections of the Fermi surface. The position of the resonances was not affected by the change in temperature.

c. Measurement of the Wave Number

When the dispersion relation for $\omega\tau=\infty$ has a real solution, we can consider the metal or semimetal to be a dielectric medium. Then we observe the intensity maxima of reflected power if the condition,

$$q_r d = \pi N, \tag{44}$$

is satisfied, where q_r is the wave number in a sample, d is the sample thickness and N is an integer. This condition corresponds to the interference of the wave reflected multiply between the plane parallel faces of the sample (Fabry-Perot interference condition). Since q_r varies as a function of magnetic fields for magnetoplasma waves (Alfven waves), a series of interference fringes is observed.

In the simplest case where the dispersion relation ($\omega_c\tau \gg \omega\tau \gg 1$) is given by

$$\frac{q_r}{\omega} = \frac{\pi}{\omega d} N = \frac{\sqrt{4\pi}}{H} \sqrt{\sum_i n_i m_i} \tag{45}$$

in the Eq.(19) and the carrier density $\sum n_i m_i$ is independent of magnetic fields, the interference appears periodically with respect to the inverse magnetic field strength as shown in Figs. 3 and 9. The marked deviation from the straight line at high field is explained in terms of the quantum variation of the energy.[12] Further, the deviation of the field lower than the second harmonic of holes is explained in terms of the coupling of the Alfven wave mode to the magneto-acoustic wave.[37-38]

d. Measurement of the Effective Mass

During each cyclotron period an electron interacts with the r.f. field for a short time compared with either the cyclotron period or the r.f. period. Resonance will occur if the electron makes each rapid traverse of the penetration depth at the same point in an r.f. period, i.e., if $\omega/\omega_c = n$ where n is a nonzero integer. At the resonance the r.f. power absorption is minimum in metals as seen in Sec.II(d). For a free electron gas and $\omega\tau > 5$ (in the Azbel'-Kaner condition), the mass value as derived from $\Delta(1/H)$ using either absorption minima or derivative maxima as the resonance criteria are in error by no more than 0.5%. While the use of the fundamental resonance alone may lead to errors as large as 10% as shown by Kip, Langenberg and Moore.[39] But these conclusions are changed rapidly in case of the weakly nonlocal condition, which we discussed in Sec. II(f). We must determine the mass value compared with the calculated line shape in Sec. VI.

V. EXPERIMENTAL RESULTS AND DISCUSSIONS

a. Holes

Figs. 4-8 show the field derivative of the surface impedance for the various configurations. Fig. 4 is obtained from the specimen of the thickness 0.715 mm with parallel planes in the configuration that $\vec{q}$ is along a binary axis, $\vec{B}$ along the bisectrix axis and $\vec{E}_{rf}$ along the trigonal axis. The Fabry-Perot interference pattern due to the Alfven waves and "Azbel'-Kaner cyclotron resonance" at the second and higher harmonics of the holes are observed. The fundamental resonance is so weak that it is masked by the interference pattern of the dimensional resonances (Fabry-Perot). These interference patterns can be solved to obtain the wave number q of the Alfven waves using the condition (44). The wave number q obtained in this manner is plotted in Figs. 9 and 10 as a function of magnetic field. The experimental points are in an excellent agreement with the solid line obtained by solving the dispersion relation in Eq. (31) for the lowest order nonlocal anisotropic dielectric functions for bismuth. We have neglected the off-diagonal elements of the dielectric tensor arising from the tilting of the electron energy surfaces, since they have very little effects for $\omega_{ce}\omega_{ch} \gg \omega^2$ on our results. The dispersion relations for the longitudinal mode ω_- and the Alfven waves in the local limit are shown in this figure as broken lines. The calculation was based on Eqs. (23) and (31). Near the second harmonic the wave length of the Alfven waves is about 15 times as large as the cyclotron radius. The coupling

of the transverse excitation with Alfven waves cannot be observed, since X is much less than one in this case. If the specimen is thick and wedge-shaped, the Fabry-Perot interference pattern disappears and only the change of the surface impedance is observed as shown in Fig. 5 because the damping (imaginary part of the wave number) near the resonance is large. We observe a weak peak near the fundamental and the absorption due to a dielectric anomaly on the low field side in addition to the cyclotron harmonics already seen in Fig. 4. As the static magnetic field is rotated from the bisectrix to the trigonal axis, the resonance line shape near the second harmonic becomes complex with a satelite peak on the low field side as shown in Fig. 7. This peak corresponds to a transverse excitation which becomes stronger with increasing X. Due to the characteristic mass anisotropy of bismuth, X near the second harmonic becomes large as the magnetic field is rotated from the bisectrix to the trigonal axis. The conditions are the same for $\vec{q}$//trigonal, $\vec{B}$//bisectrix and $\vec{E}_{rf}$// binary axis. Fig. 8 shows the line shape in the vicinity of the second harmonic for this configuration. Since X near the resonance is still larger than that in Fig. 5, the peaks due to the "transverse" and "longitudinal" resonance separate further as shown by arrows. For the ordinary mode where $\vec{E}_{rf}$ is parallel to the magnetic field, the fundamental cyclotron resonance is stronger than the second harmonic as shown in Fig. 6. In this magnetic field direction, the crystal symmetry is poor and the extraordinary mode is not totally excluded. Consequently the

oscillatory variation of the reflected power due to the interference of Alfven waves is observed in this orientation as well. The absorption is due to the transverse waves which are called high frequency waves for the ordinary configuration.[32)]

b. Electrons (Cyclotron Resonance)

Figs. 11-13 show the field derivative of the surface impedance for various configurations. Resonance patterns were observed as the magnetic field was changed cyclically from positive to negative values as shown in the upper part of Fig. 11. In the middle part of Fig. 11 the magnetic field values of the peak positions of the cyclotron harmonics are sketched as a function of reciprocals of the harmonic order in the configuration that q//binary, B//bisectrix, and E_{rf}//trigonal axis. The curve displays a hysteresis loop just as is observed in ferromagnetism. As the magnetic field cyclically decreased, the curve becomes linear with practically no change in slope at the origin. Further, the magnetic field is changed from positive to negative direction passing through the zero, and then the cyclotron resonances at low magnetic fields have fickle structures and are weak. In this case the internal total magnetic fields don't change smoothly. On the other hand, when the magnetic fields are changed many times on one side or decreased, the internal total magnetic fields are about ten gauss and nearly constunt. The line shape is smooth and depend only on the change of the applied magnetic fields. Similar hysteresis curves are obtained for other magnetic field directions. The reasons why the hysteresis appears in electron cyclotron resonances are not clear, but we will speculate them. They are as follows;

1. some ordered states due to the superconducting state of the surface layer because the amorphous thin film of bismuth is superconductor ($T_c \sim 6^{\circ}K$, $H_c \sim 430g$), [40]

2. paramagnetic behaviour of the surface skipping electrons. In the case 1, there is no physical interpretation to persuade. In the case 2, the surface states are few in number, and their number is proportional to sample perimeter rather than area, yet because they produce circulating currents all along the edges they have a huge paramagnetic moment which increases with sample size. They form a virtually unquantized continuum of levels which are extremely sensitive to changes in H, for any such change induces a circulating electric field which acts powerfully upon the surface current.[41] Let us now consider the skipping electrons discussed in Sec. II(g). The transitions between these quantized levels are observed in Fig. 21 and ref. 18. A surface current density $J = nx_n ev_F$ is associated with this surface state, x_n, n, and v_F are the penetration depth of the surface state, the carrier density, and the Fermi velocity in the direction of the surface current, respectively. The surface current produces a magnetic field in the bulk of a metal with the direction so as to enhance the applied magnetic field. The magnitude of the enhanced magnetic field is given by

$$H' = 4\pi J/c = 4nev_F x_n/c \,. \qquad (46)$$

The thickness of the surface state is given by Eq.(37). If we put $H' = H$ in this equation, we get a self consitent magnetic field

$$H = \left(\frac{8}{9}\right)^{1/2}\left(\frac{4\pi ne v_F}{c}\right)^{3/4}\left(\frac{ck^2}{2e\rho_F}\right)^{1/4}. \qquad (47)$$

Assuming that $n=3\cdot10^{17}cm^{-3}$, $v_F \cong 10^8 cm/sec$, we get $H \cong 100$ gauss. But according to Kubo[42] the energy levels of the surface electrons

become higher than the electrons in the bulk or skimming electrons, and therefore the Landau diamagnetism is correct. But it was shown that the skipping electrons contributed to the paramagnetism and the susceptibility is given by[43]

$$\chi = -V \frac{n\mu^2}{2E_F} + A \frac{n\mu^2}{2E_F} \frac{9}{62} \left(\frac{2\pi^2 k^2}{m E_F} \right)^{1/2} \qquad (48)$$

where μ, V, and A are $\frac{e\hbar}{2mc}$, the volume of a sample and the surface area, respectively. In bismuth, $m^* \sim 0.001 m_o$, $E_F \sim 25$meV, then $V/A \sim 10^{-6}$cm. If the thickness of a sample or certain domains was thinner than 10^{-6}cm, the paramagnetic property would appear.

For determination of mass values from these experiments, it is quite important to take into account of this hysteresis effect. In Figs. 12 and 13 the strength of the higher harmonic cyclotron resonance decreases rapidly as the harmonic order increases. For the ordinary mode the cyclotron resonances have more complicated structures than for the extraordinary mode. The line shape of the cyclotron resonance in Figs. 12 and 13 will be discussed in the followin section.

VI. CALCULATION OF LINE SHAPE OF CYCLOTRON RESONANCE AND DISCUSSIONS IN BISMUTH

In this section we shall calculate the line shape of the reflection or the absorption of the microwaves in terms of the surface impedance and compare the calculated line shapes with the experimental results presented in Sec. V. Hebel dicussed the microwave absorption due to a slightly anomalous skin effect by calculating the surface conductivity and refractive index from the dispersion relation for the weakly nonlocal case.[8] His method is applicable both for difuse and specular reflection, unfortunately it is limited to the ordinary mode and to the extremely weakly nonlocal case where $R \ll 1/|q|$, and the difference between the specular and diffuse is little. Therefore we have employed the standard method of calculating the surface impedance, which has been extensively used in metals, but we have considered both the long and short wavelength approximations. In the case of metals the density of carriers is so high that $|q|R \gg 1$, and the dielectric functions can be expanded asymptotically in terms of $1/qR$. In this case the integrand of Eq. (7) has no pole in the region of long wavelength, and can be analytically integrated as was done by Azbel'-Kaner[15] and other authors.[23,44] For bismuth, however, the carriers are compensated and their densities are so low that the integrand has poles in the region of long wavelength for an infinite relaxation time. In Fig. 14 the result of the calculation for the second harmonic is compared with the experiment in the configuration; $\vec{q}$//binary, $\vec{B}$//bisectrix and

$\vec{E}_{rf}$//trigonal axis. In this calculation only the lowest order terms (X^2) were taken into account but the result depends negligibly upon the upper limit of the integration and the higher order terms for this second harmonic. The transverse resonance at the second harmonic appears but is very weak as shown in Fig. 15. For the third harmonic shown in Fig. 15 the convergence is very poor and is sensitive to the higher order terms, since the Alfven waves couple with the longitudinal or transverse mode at $qR \sim 1$ around the third harmonic. When $qR > n$, the asymptotic formula is correct as discussed in Sec. II(d) but the coupling occurs in the region where $qR < n$. Therefore, for the integration from 0 to $4/R$, the integrand was expanded up to X^{20}, and for that from $4/R$ to infinity, the asymptotic formula was employed. The result reproduces the experimental curve fairly well, when we assumed that $\omega\tau = 100$. This relaxation time coincides with the obtained one for the dispersion relation.

When $\vec{q}$//trigonal, $\vec{B}$//bisectrix and $\vec{E}_{rf}$//binary axis, qR is nearly equal to unity in the neighbourhood of the second harmonic due to the anisotropy of the hole mass. In this case the transverse and the longitudinal excitations are clearly separated. The result of the calculation for the surface impedance is shown in Fig. 16, which should be compared with the observed derivative curve shown Fig. 8. The arrows in Figs. 2 and 8 are the "transverse" and "longitudinal" resonances, respectively (points A and B). The field intervals delineated by arrows on the experimental and calculated curves agree very well (see Figs. 8 and 16). However,

the experimental relative intensity of these two peaks is reversed from the calculated intensity. Although the peak for the transverse resonance of the experiment is stronger, the high field edge (B) of the absorption curve is steeper than the low field edge (A) in the calculation. This discrepancy probably results both from the failure of the assumption that the carriers reflect specularly at the surface, and the neglect of the off-diagonal elements, arising from the tilting effect of the electron Fermi surfaces, of the dielectric tensor because in this case the cyclotron resonance is near the hybrid resonance. If we attribute the series of anomalies in the reflection curve to the harmonics of the Azbel'-Kaner cyclotron resonance, we obtain the value (0.213 $\pm$0.002)m_o as the cyclotron mass for holes for $\vec{B}$//bisectrix axis. However, according to the above discussion, we analyze the line shape including the shift of peaks from the position of the exact cyclotron harmonics. The mass value determined in this manner is (0.210$\pm$0.002)m_o. The difference between these two masses is greater than one standard deviation.

When the polarization of the microwaves is rotated from the extraordinary to ordinary configuration, the centre of the anomaly at the second harmonic shifts to the higher field side as shown in Fig.17. Since the transverse resonance dominant in the ordinary configuration is on the lower field side compared with the longitudinal resonance which is dominant for the extraordinary configuration at the weakly nonlocal limit, the resonace would shift to the lower field side with rotation of the microwave polarization if the cyclotron mass were constant. So we

have concluded that the limiting point mass which is responsible for the resonance in the ordinary configuration is larger than the mass of the extremum orbit. The limiting point mass was estimated to be $(0.217\pm0.003)m_o$ for $\vec{B}$//bisectrix from this experiment. The mixing of the extraordinary mode in the ordinary configuration can be neglected for the cyclotron resonance, since the calculated line shape for the pure ordinary mode as shown in Fig. 18 agrees with the experimental curve shown in Fig.6.

Finally we discuss the cyclotron resonance of electrons. The coupling of the electromagnetic waves with the longitudinal or transverse excitations occurs in the region where $X\sim3n$ for $\vec{B}$// bisectrix. For the calculation of the surface impedance, the functions in the integrand were expanded up to X^{20} for the integration with respect to q from 0 to 10/R, and the asymptotic formulas were employed for that from 10/R to infinity. In Fig. 19, the result of the calculation for the extraordinary configuration ($\vec{q}$//binary, $\vec{B}$//bisectrix) is shown. This is to be compared with the experimental curve in Fig. 12. In Fig. 19 the positions of the resonances for the light electrons, the heavy electrons and the electron-electron hybrid are indicated with le, he and e-ehy, respectively ($m_{le}=0.0091m_o$, $m_{he}=0.0196m_o$). The real part of the surface impedance, which is proportional to an absorption, has structure near the each resonance and the peaks are at the field higher than the each resonance, but the experimental is simple (Fig. 12) therefore the relaxation time and the homogenity of the low magnetic field is not so good as assumed in the calculation. On the other hand, the absorption peaks for the ordinary configuration occur at

each electron cyclotron resonance as shown in the calculation for the holes in Fig. 18. The experimental result is shown in Fig.13. This curve is more complicated than the curve for the extraordinary mode in Fig. 12. The strength of the higher harmonic cyclotron resonances decreases rapidly as the harmonic order increases for both configurations. The extra-structure in the ordinary configuration is due to the combined resonances. The spin splitting factor is the same as obtained by Smith, Baraff and Rowell[45] from magnetoresistance measurements, but the resolution is worse than their experiment. Further it is difficult to understand why the hybrid resonance for the extraordinary configuration is weaker than the ordinary configuration as shown in Figs. 12 and 13. One of the reasons may come from neglect of the tilting of electron Fermi surfaces in the calculation. The eigen-modes become mixtures of ordinary and extraordinary modes due to the tilting of the electron energy surfaces. In practice, the electron-hole hybrid resonance is sensitive to the neglect of the tilting effect of the electron energy surfaces.

Taking into account of the difference of assignment of resonance points for the extraordinary and ordinary configurations as discussed above, we obtained the cyclotron masses of electrons at extremum orbit (extraordinary) as well as limiting point (ordinary) as shown in Table 1. The effect of hysteresis was assumed to give a constant shift of magnetic field.

For some crystal orientation we observed high frequency waves as shown in Fig.20. Some of the magnetic surface state resonances were observed for B//bisectrix axis as shown in Fig. 21.

This structure is the same as the observed one in ref. 18.

The line shapes and the strength of the cyclotron resonances, and the surface state resonances are sensitive to the surface conditions. But the dielectric anomaly and hybrid resonance are insensitive. Even when we could not observe the surface states though the surface were fresh, we used the same relaxation time as determined from the low field magnetoresistance,[46] the wave number of the coupled modes in Fig. 10 and from the line shape of the interference patterns due to the Alfven waves,[12] in order to analyse the line shape. At the low magnetic field the relaxation time becomes short. Rather nice fit of the line shape between theory and experiment shows that the relxation time of the surface and the bulk are almost equal for cyclotron resonances.

CONCLUSIONS

The cyclotron resonance in bismuth is understood in terms of the coupling of electromagnetic waves with a longitudinal magnetoplasma excitation and a transverse excitation. Considering on the line shape of the calculation, we determine the cyclotron effective mass. (Table 1)

Appendix A (Conductivity)

Let us now consider the case of an ellipsoidal and parabolic dispersion which is defined in the Cartesian ordinate (0123) by the equation:

$$2E m_0 = \alpha_1 P_1^2 + \alpha_2 P_2^2 + \alpha_3 P_3^2 + 2\alpha_{12} P_1 P_2 + 2\alpha_{23} P_2 P_3 + 2\alpha_{31} P_3 P_1 .$$

The cyclotron mass M_c for B along the 03 axis is

$$M_c = m_0 / (\alpha_1 \alpha_2 - \alpha_{12})^{1/2} ,$$

the ellipsoid volume V in momentum space is

$$V = \frac{4\pi}{3} (2 E_F m_0)^{3/2} \Big/ \begin{vmatrix} \alpha_1 & \alpha_{12} & \alpha_{31} \\ \alpha_{12} & \alpha_2 & \alpha_{23} \\ \alpha_{31} & \alpha_{23} & \alpha_3 \end{vmatrix} = \frac{4\pi}{3} (2 E_F m_0)^{3/2} / D^{1/2} ,$$

and the carrier density then reads

$$n = \frac{2}{h^3} V .$$

When the magnetic field is not along a principal axis of the ellipsoid, the real space trajectory is the resultant of a uniform motion along the magnetic field and of an elliptical trajectory in a plane perpendicular to the field. The velocity components and the momentum component p_z are ($\phi = \omega_c t$)

$$v_1 = (2\alpha_1 E_F/m_0)^{1/2} \sin\theta \cos(\phi - \phi_d)$$

$$v_2 = (2\alpha_2 E_F/m_0)^{1/2} \sin\theta \sin\phi$$

$$v_3 = (2\eta E_F/m_0)^{1/2} \cos\theta + \mu v_1 + \nu v_2$$

$$\cos\phi_d = (1 - \alpha_{12}^2/\alpha_1\alpha_2)^{1/2}, \quad \sin\phi_d = \alpha_{12}/(\alpha_1\alpha_2)^{1/2},$$

$$p_z = (2 E_F/m_0)^{1/2} \cos\theta$$

where $$\eta = \begin{vmatrix} \alpha_1 & \alpha_{12} & \alpha_{31} \\ \alpha_{12} & \alpha_2 & \alpha_{23} \\ \alpha_{31} & \alpha_{23} & \alpha_3 \end{vmatrix} \Big/ (\alpha_1\alpha_2 - \alpha_{12}^2) ,$$

$$\mu = (\alpha_2\alpha_{13} - \alpha_{23}\alpha_{12}) / (\alpha_1\alpha_2 - \alpha_{12}^2),$$

and $$\nu = (\alpha_1\alpha_{23} - \alpha_{13}\alpha_{12}) / (\alpha_1\alpha_2 - \alpha_{12}^2).$$

Comparing the expressions for M_c, n, p_z, v_1, v_2, and v_3 with the similar expressions in ref. 28 for the spherical case, we obtain the conductivity tensor in terms of the tensor σ^s with angular frequency ω_c and spatial exploration parameter X relevant to the considered ellipsoid.

$$\omega_c = \frac{eB}{M_c C} \quad , \quad X = qR = q_y (2\alpha_2 E_F / m_c)^{1/2} / \omega_c$$

$$\sigma_{11} = \alpha_1 \left(\cos^2\phi_d \, \sigma_{11}^s + \sin^2\phi_d \, \sigma_{22}^s \right),$$

$$\sigma_{22} = \alpha_2 \, \sigma_{22}^s ,$$

$$\sigma_{12} = (\alpha_1\alpha_2)^{1/2} \left(\cos\phi_d \, \sigma_{12}^s + \sin\phi_d \, \sigma_{22}^s \right),$$

$$\sigma_{21} = (\alpha_1\alpha_2)^{1/2} \left(\cos\phi_d \, \sigma_{21}^s + \sin\phi_d \, \sigma_{22}^s \right),$$

$$\sigma_{33} = \eta \, \sigma_{33}^s + \mu^2 \sigma_{11} + \nu^2 \sigma_{22} + \mu\nu \left[\sigma_{12} + \sigma_{21} \right],$$

$$\sigma_{13} = \mu \sigma_{11} + \nu \sigma_{12} ,$$

$$\sigma_{31} = \mu \sigma_{11} + \nu \sigma_{21} ,$$

$$\sigma_{23} = \mu \sigma_{21} + \nu \sigma_{22} ,$$

$$\sigma_{32} = \mu \sigma_{12} + \nu \sigma_{22} .$$

Appendix B (Cyclotron Mass)

If we assume the effective mass tensor is given by

$$\overleftrightarrow{m}^* = \begin{pmatrix} m_{11} & m_{12} & m_{13} \\ m_{12} & m_{22} & m_{23} \\ m_{13} & m_{23} & m_{33} \end{pmatrix} .$$

The cyclotron effective mass is determined by[47]

$$\det\left(\overleftrightarrow{m}^*\right) + \vec{b}\cdot\overleftrightarrow{m}^*\cdot\vec{b} = 0$$

where $\vec{b} = \frac{e\vec{H}_0}{m_0 c}\frac{1}{i\omega}$ and $\vec{H}_0$ is a resonance field for electromagnetic waves of frequency ω.

TABLE 1. CYCLOTRON EFFECTIVE MASS

a. Hole

	H//trigonal axis	H//binary axis	H//bisectrix axis	
present	0.0618±0.0005 m_o	0.210±0.002 m_o	0.210±0.002 m_o	(extremum)
	0.0635±0.0005 m_o	0.217±0.003 m_o	0.217±0.003 m_o	(limiting)
Khaikin et al.[5]	0.0630 m_o	0.203 m_o	0.203 m_o	(extremum)
	0.0640 m_o	0.210 m_o	0.210 m_o	(limiting)
Kao [4]	0.067 m_o	0.226 m_o	0.226 m_o	

b. Electron

	H//3	H//2	H//1//binary axis		tilt angle
present	0.089±0.006 m_o	0.0087±0.0003 m_o	0.123±0.003 m_o	(extremum)	$6^\circ \pm 15'$
	0.113±0.006 m_o	0.0083±0.0003 m_o	0.137±0.006 m_o	(limiting)	
Khaikin et al.[5]	0.086 m_o	0.0081 m_o	0.120 m_o	(extremum)	$6^\circ 15'$
	0.117 m_o		0.137 m_o	(limiting)	
Kao [4]	0.11 m_o	0.0091 m_o	0.14 m_o		6°

The axes indicated by 1, 2, and 3 are the principal axes of the elipsoidal electron Fermi surfaces. The angle between 3 and trigonal axis is 6 degrees.

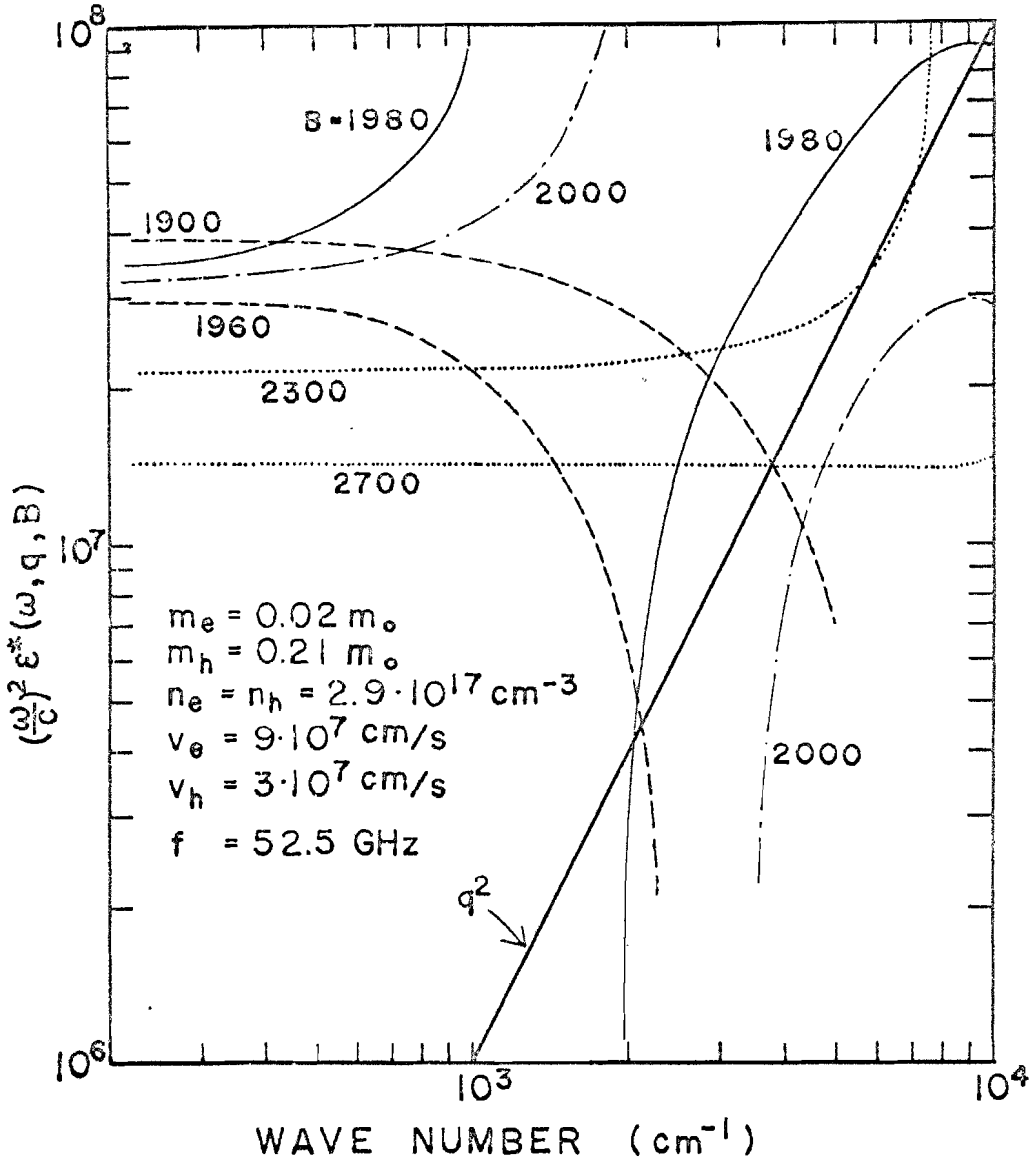
10^8
10^7
10^6
10^3
10^4
B=1980
1900
1960
2300
2700
2000
1980
2000
$m_e = 0.02\ m_o$
$m_h = 0.21\ m_o$
$n_e = n_h = 2.9 \cdot 10^{17}\ cm^{-3}$
$v_e = 9 \cdot 10^7\ cm/s$
$v_h = 3 \cdot 10^7\ cm/s$
$f = 52.5\ GHz$
q^2
$(\frac{\omega}{c})^2 \varepsilon^*(\omega, q, B)$
WAVE NUMBER (cm^{-1})

Fig. 1

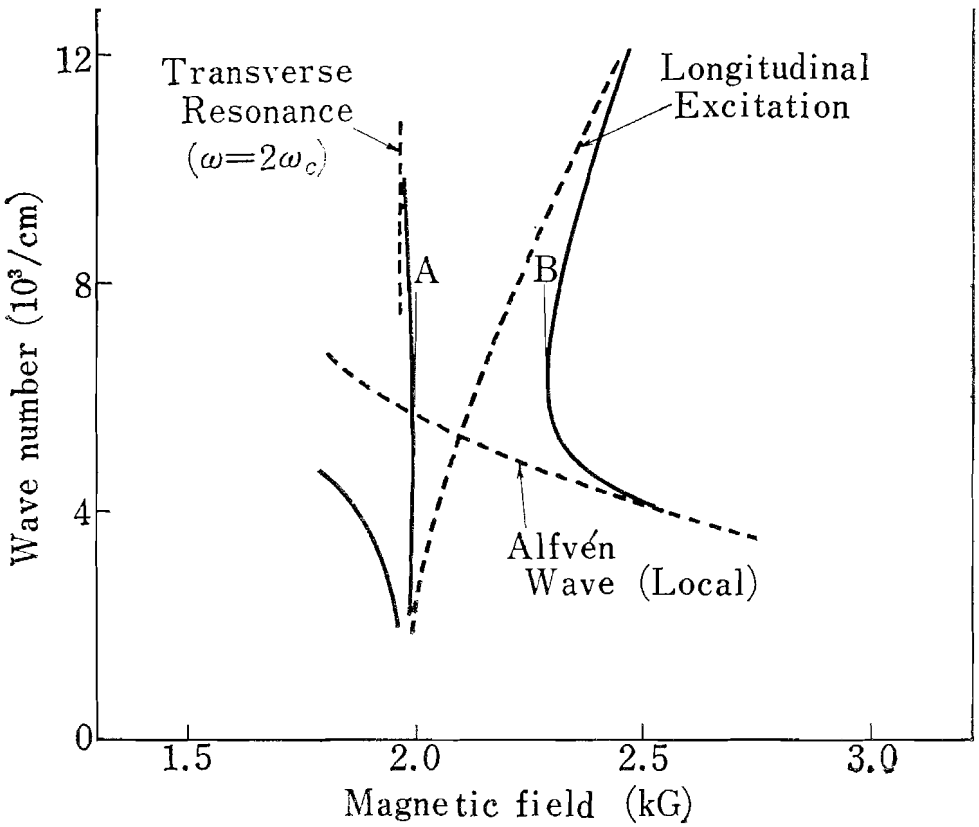
Transverse
Resonance
($\omega=2\omega_c$)
Longitudinal
Excitation
A
B
Alfvén
Wave (Local)
Wave number (10^3/cm)
12
8
4
0
1.5
2.0
2.5
3.0
Magnetic field (kG)

Fig. 2

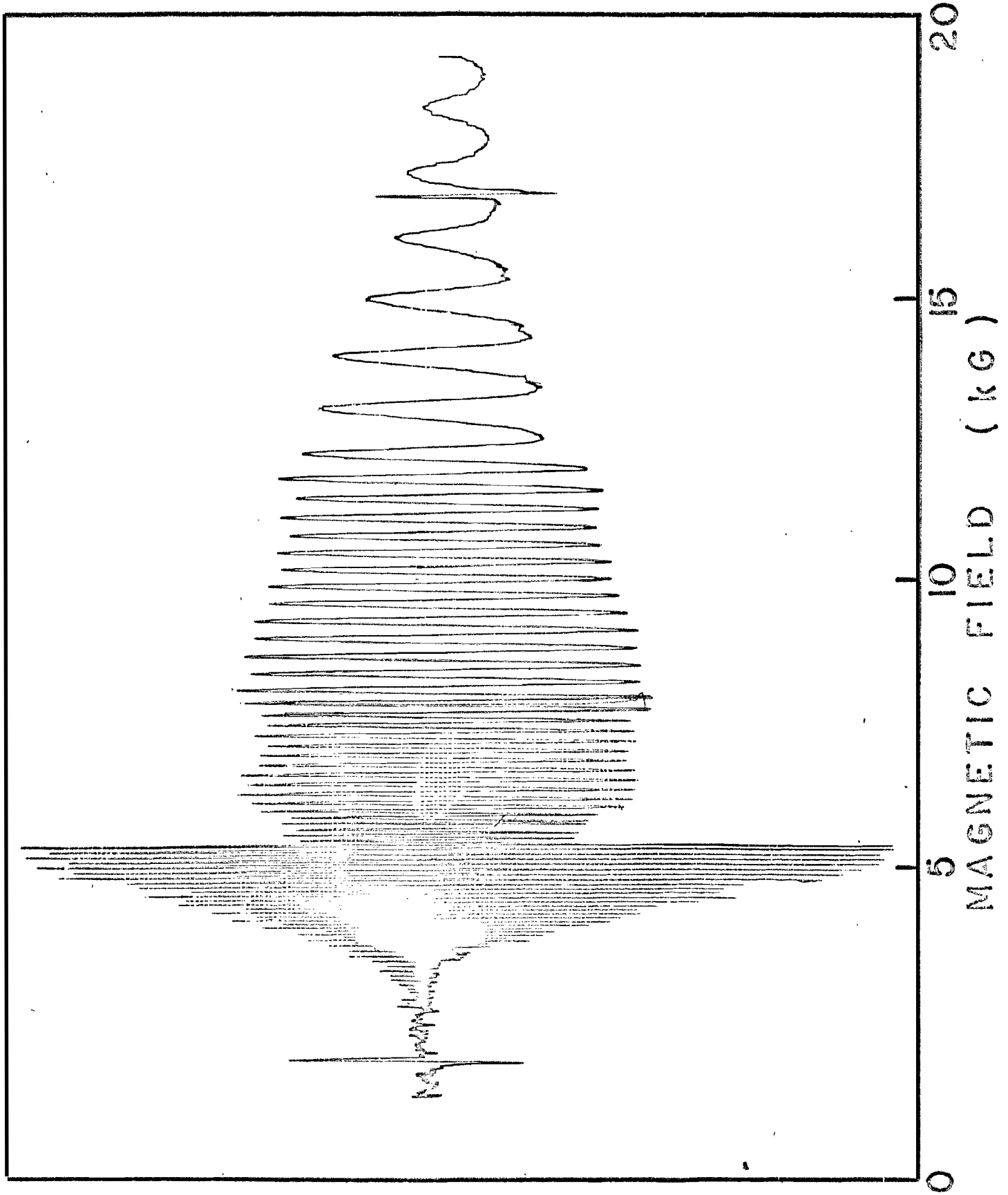

Fig. 3

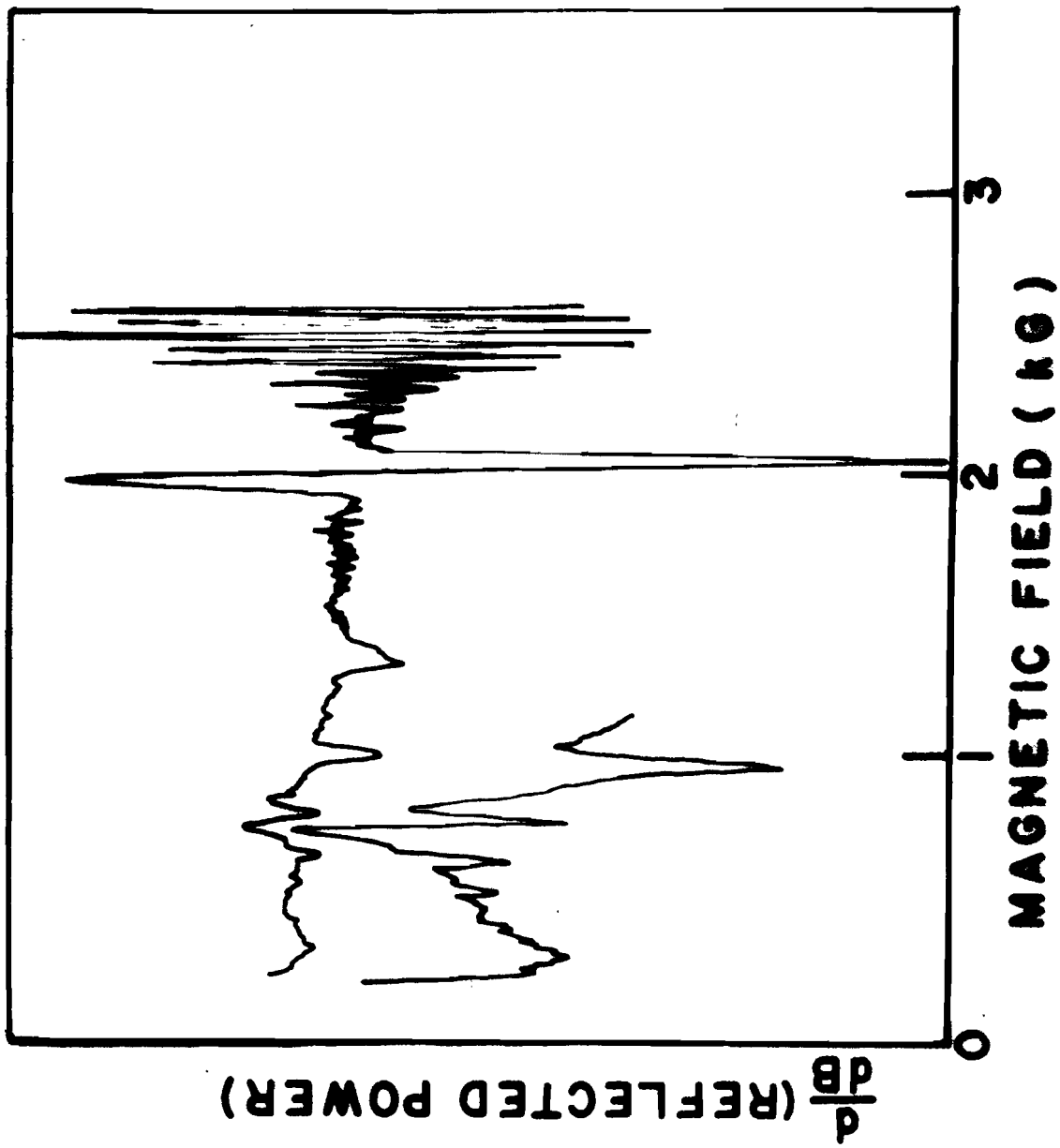

Fig. 4

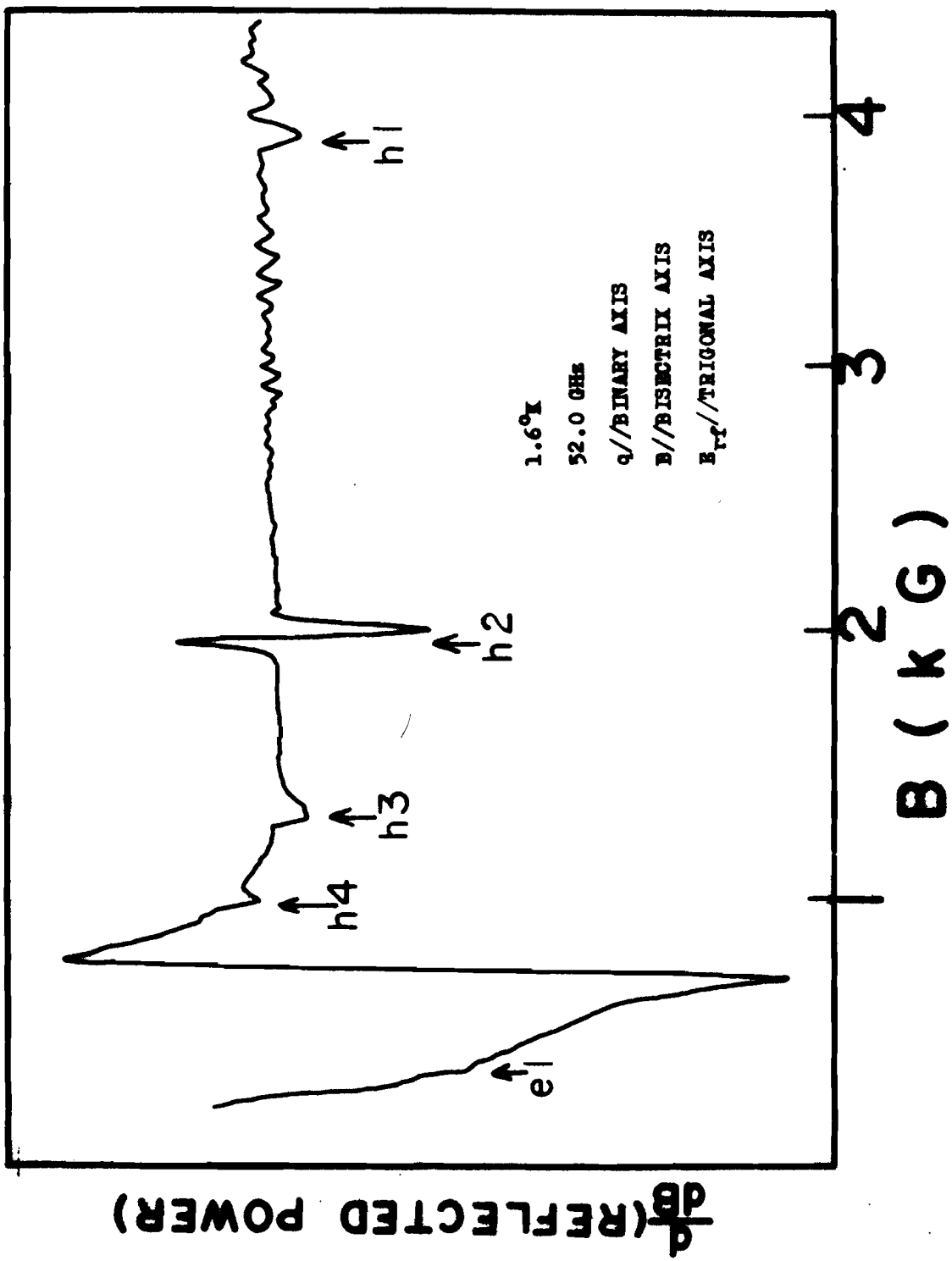
h1
h2
h3
h4
e1
1.6°K
52.0 GHz
q//BINARY AXIS
B//BISECTRIX AXIS
E_rf//TRIGONAL AXIS
1
2
3
4
B (kG)
dP/P (REFLECTED POWER)

Fig. 5

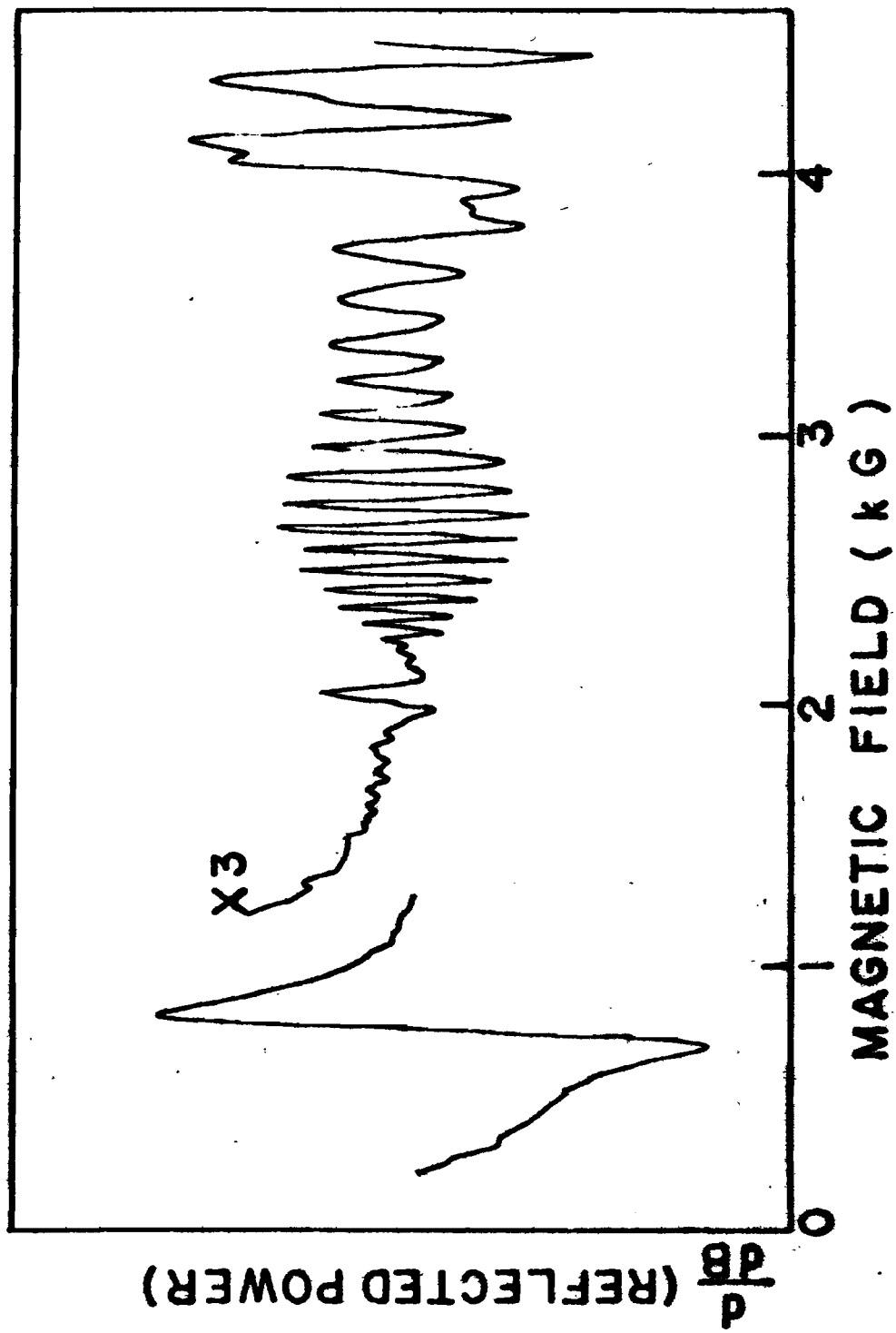

Fig. 6

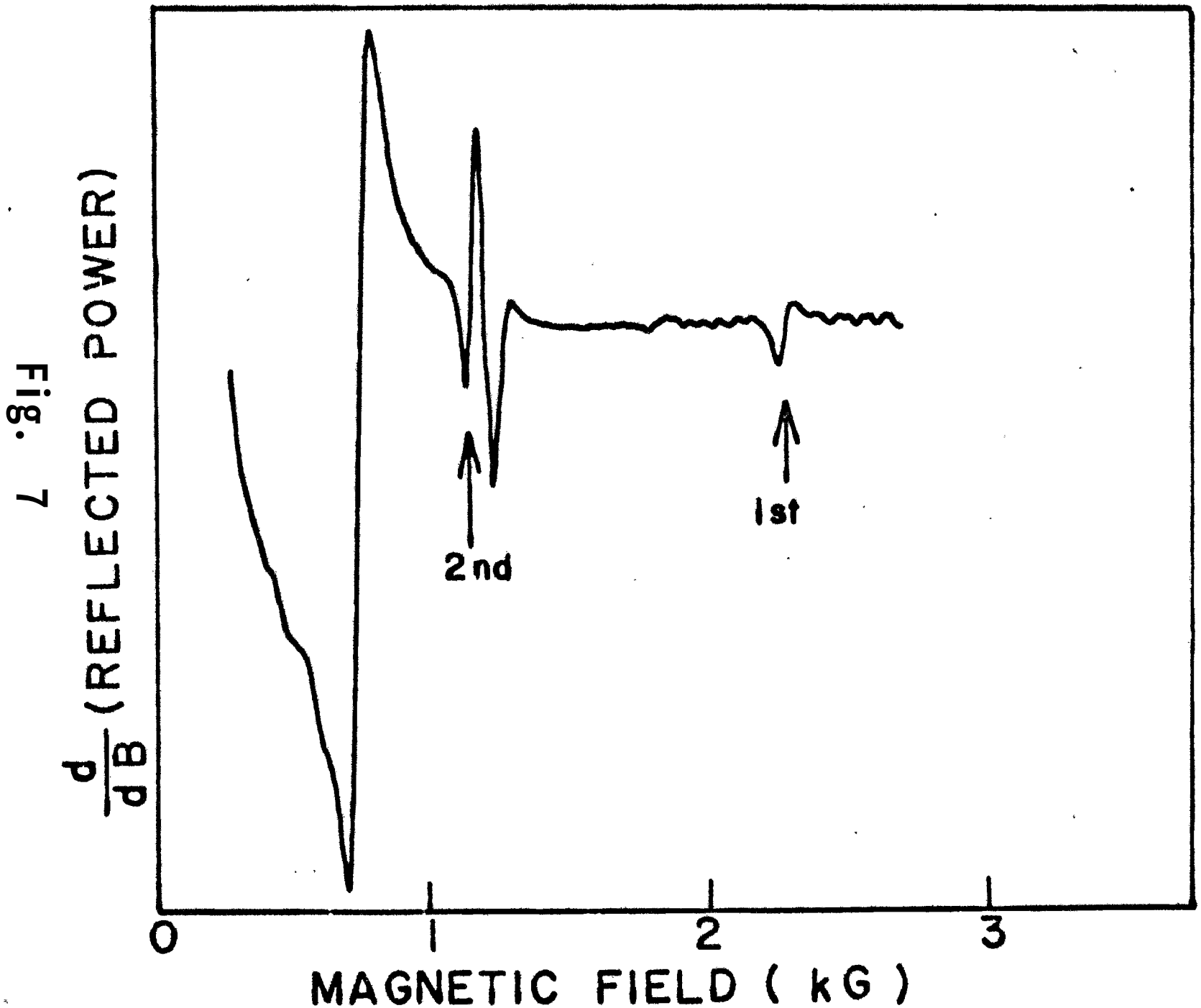

Fig. 7

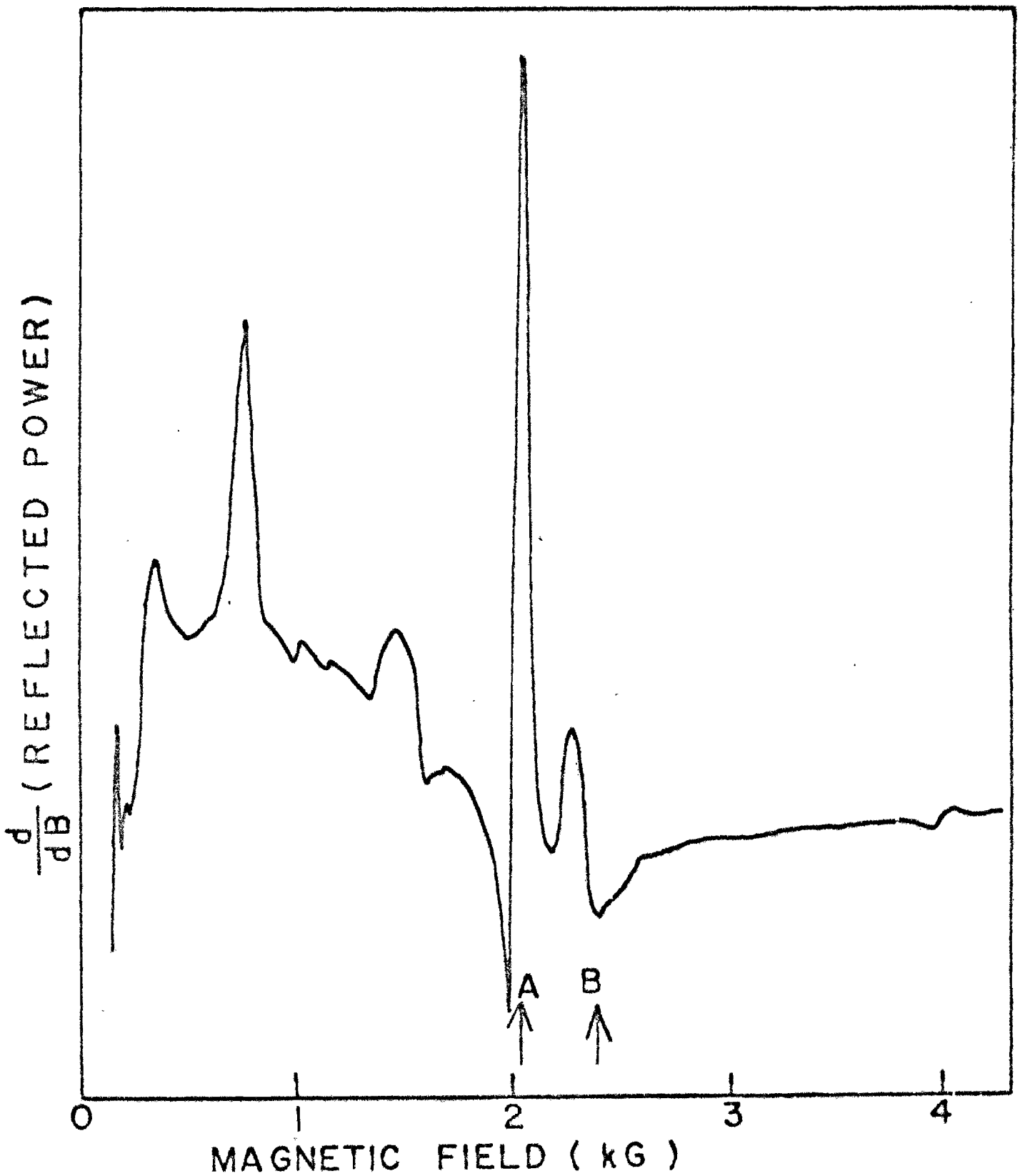

Fig. 8

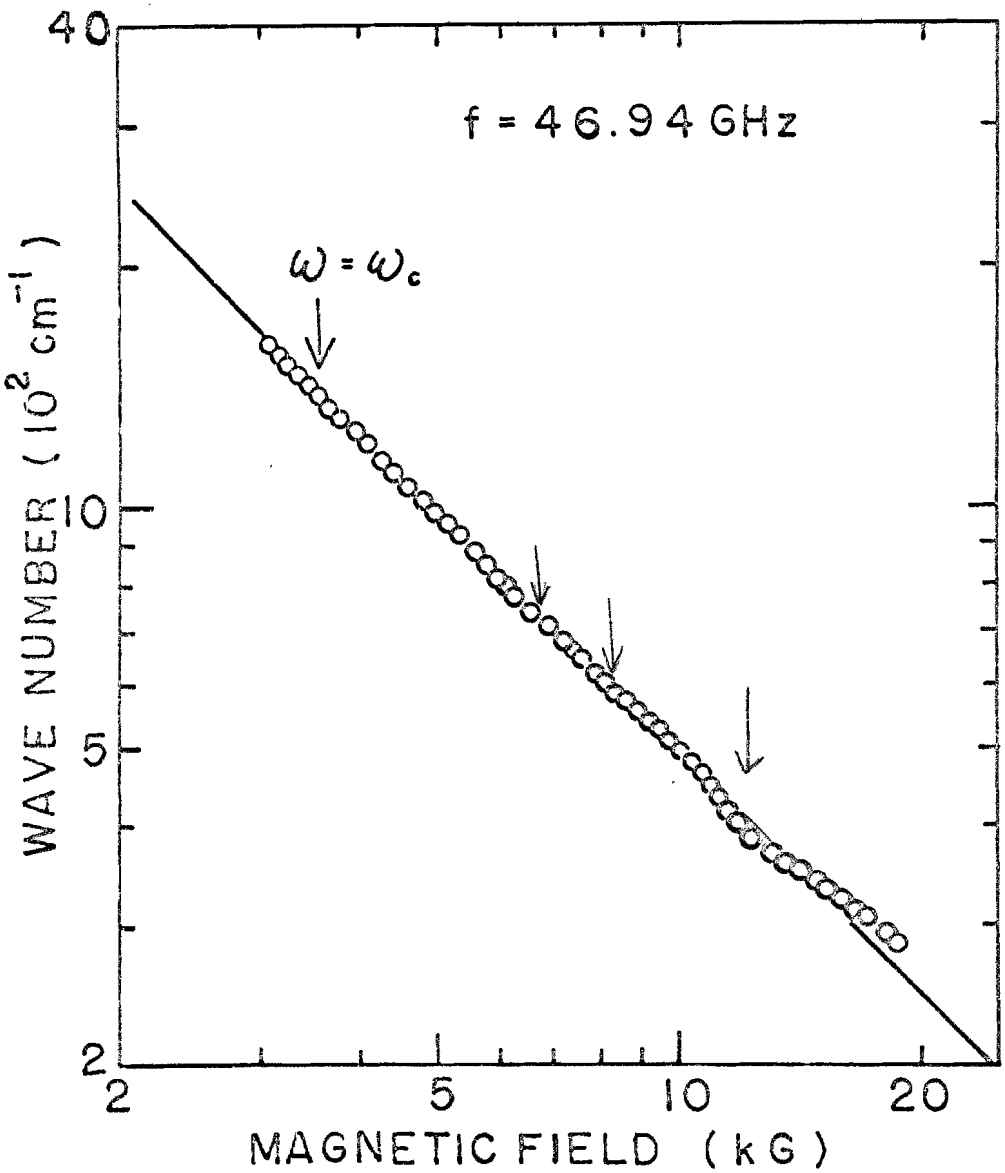
40
10
5
2
2
5
10
20
f = 46.94 GHz
ω = ω_c
WAVE NUMBER (10^2 cm^-1)
MAGNETIC FIELD (kG)

Fig. 9

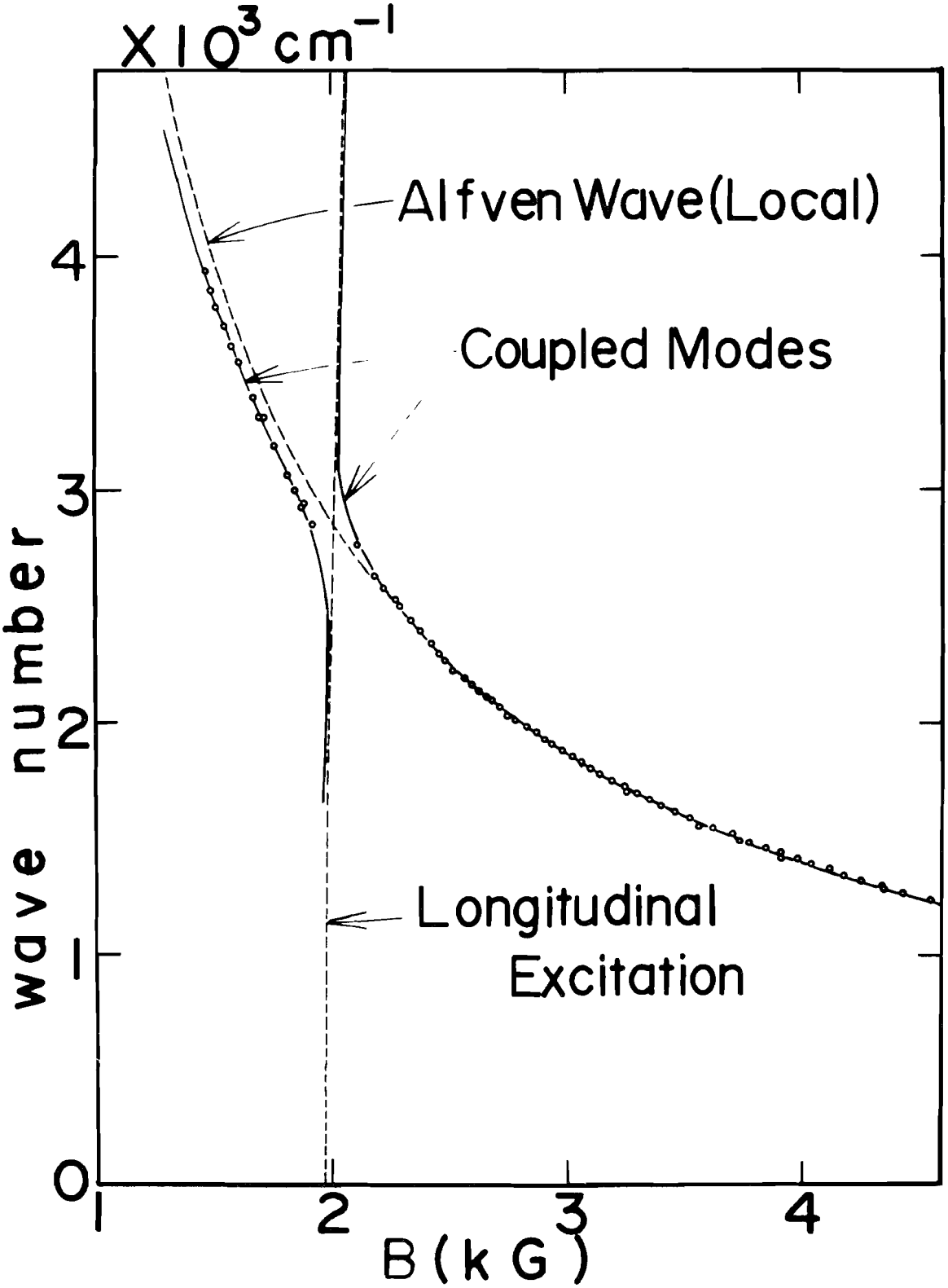
X 10³ cm⁻¹
Alfven Wave(Local)
Coupled Modes
Longitudinal
Excitation
wave number
0
1
2
3
4
B (k G)

Fig. 10

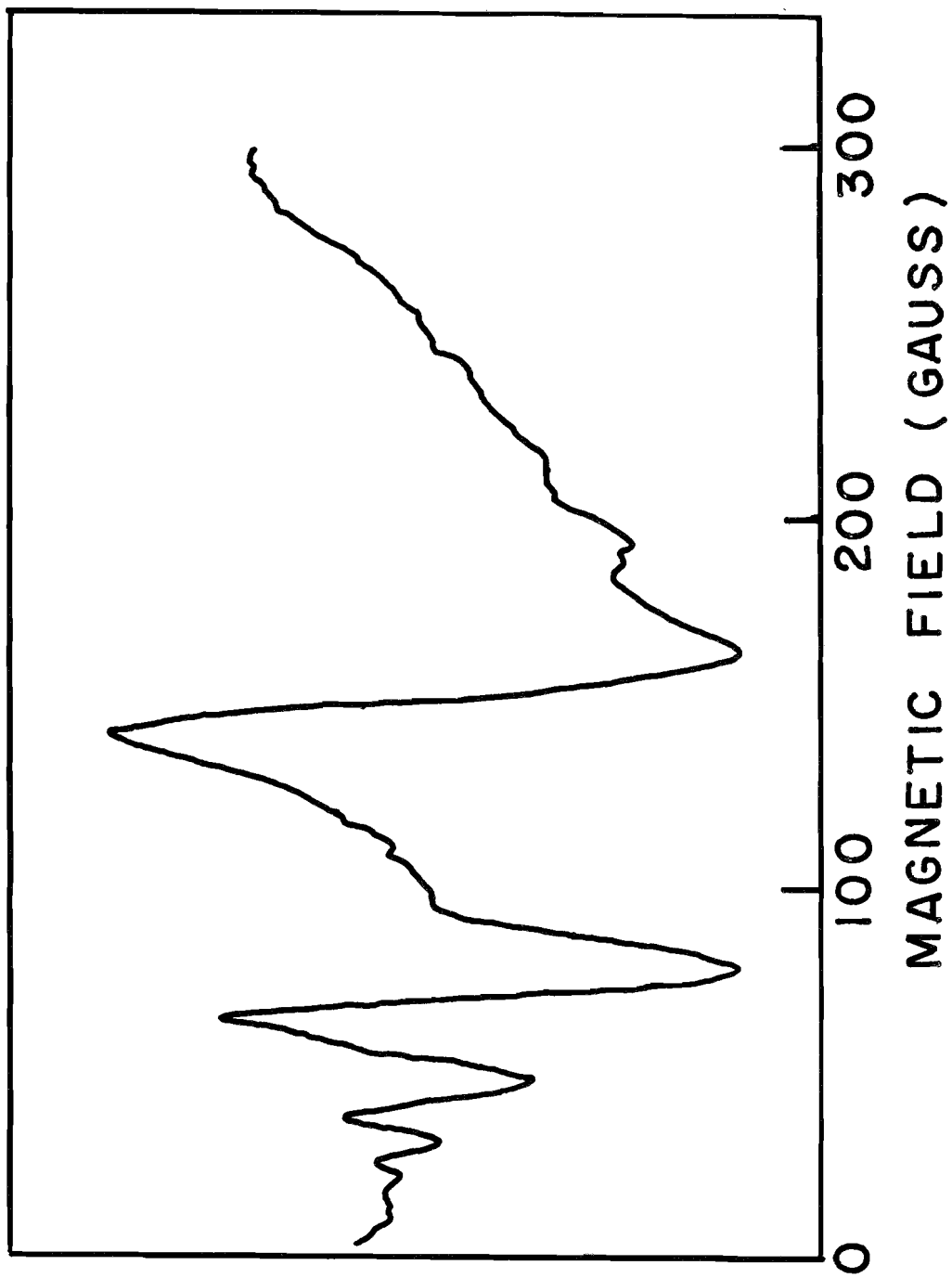

Fig. 12

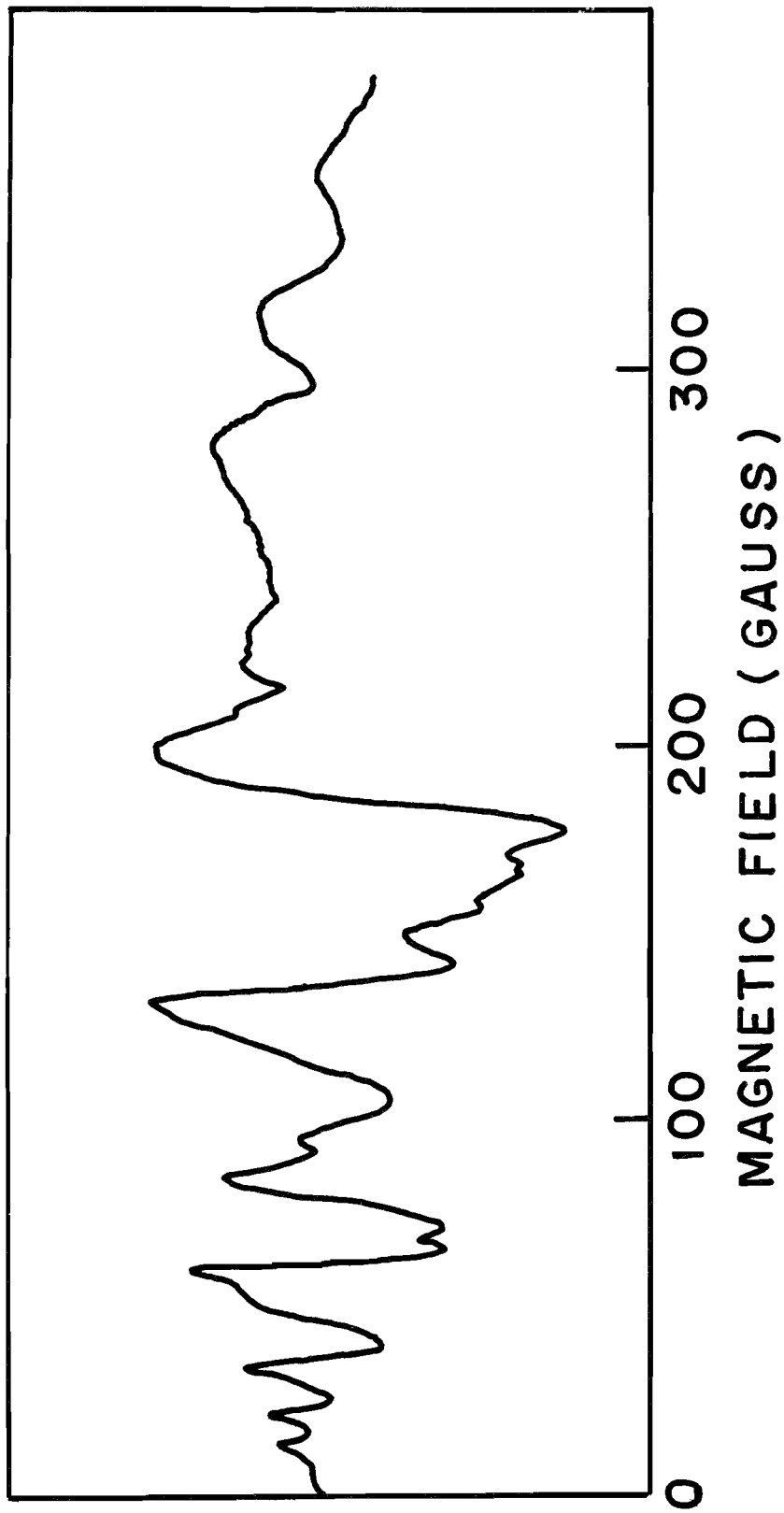

Fig. 13

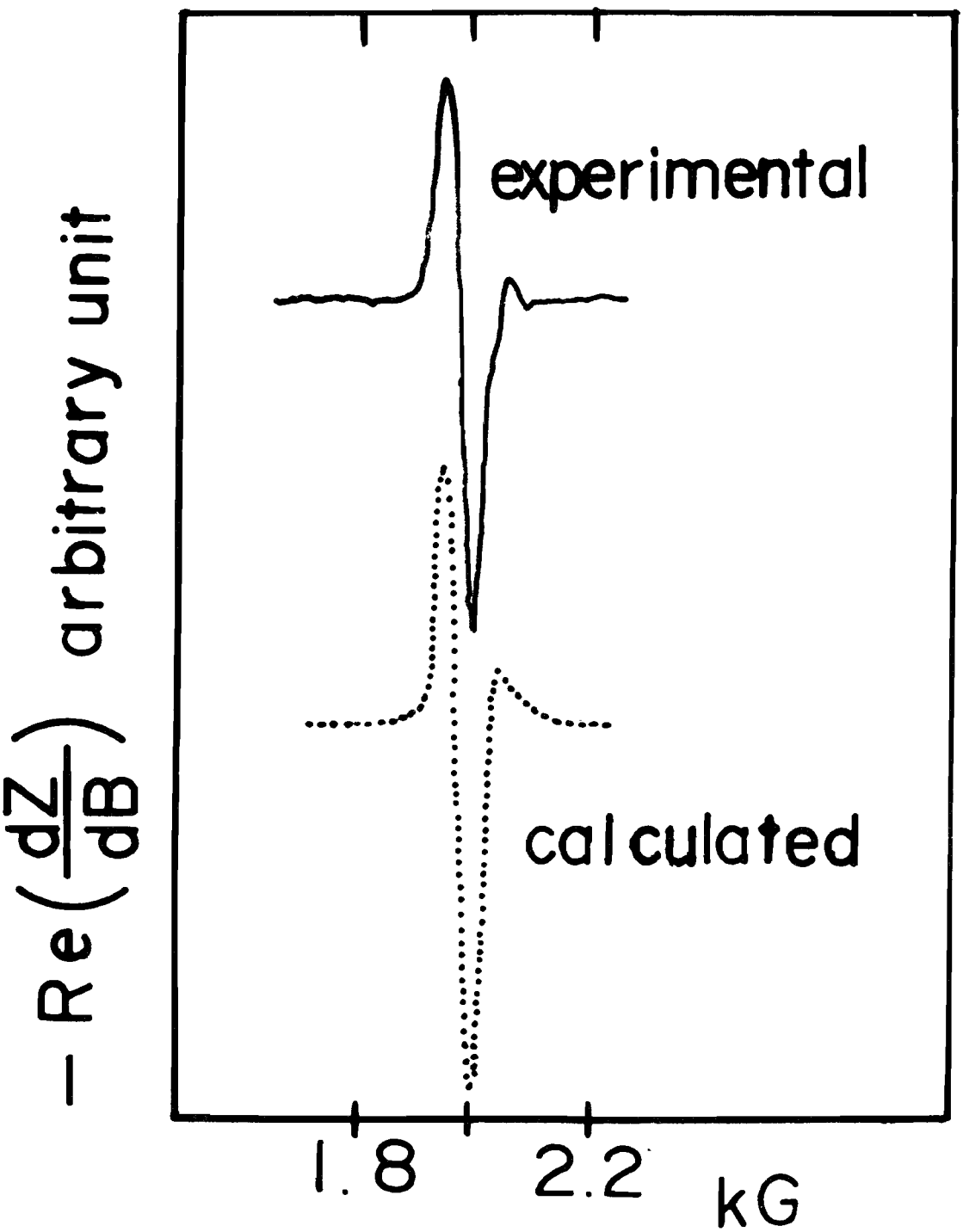
experimental
calculated
$-Re\left(\frac{dZ}{dB}\right)$ arbitrary unit
1.8
2.2
kG

Fig. 14

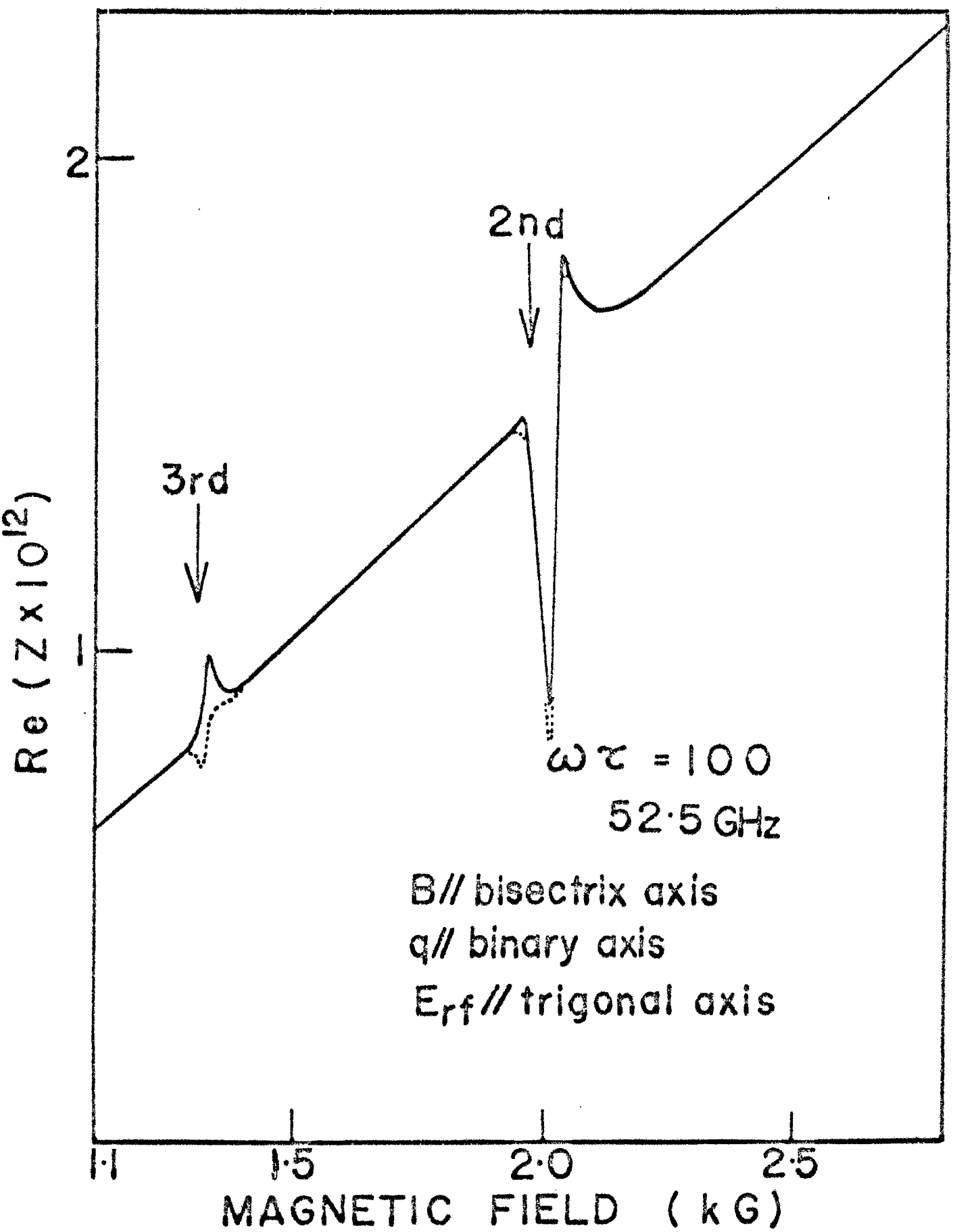
2
1
Re (Z x 10^12)
2nd
3rd
ωτ = 100
52·5 GHz
B// bisectrix axis
q// binary axis
E_rf // trigonal axis
1·1
1·5
2·0
2·5
MAGNETIC FIELD (kG)

Fig. 15

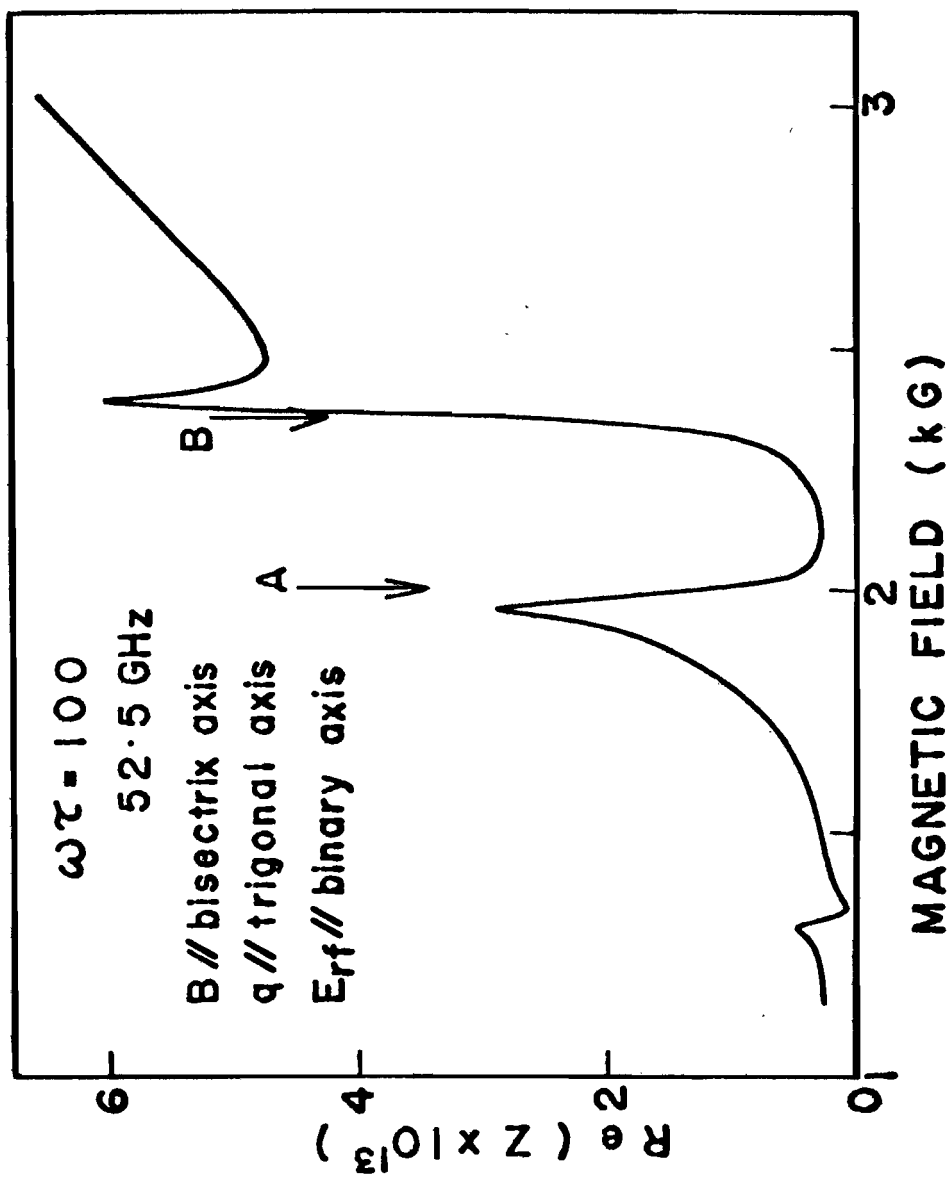
ωτ = 100
52·5 GHz
B // bisectrix axis
q // trigonal axis
E_rf // binary axis
A
B
Re (Z x 10^13)
0
2
4
6
1
2
3
MAGNETIC FIELD (kG)

Fig. 16

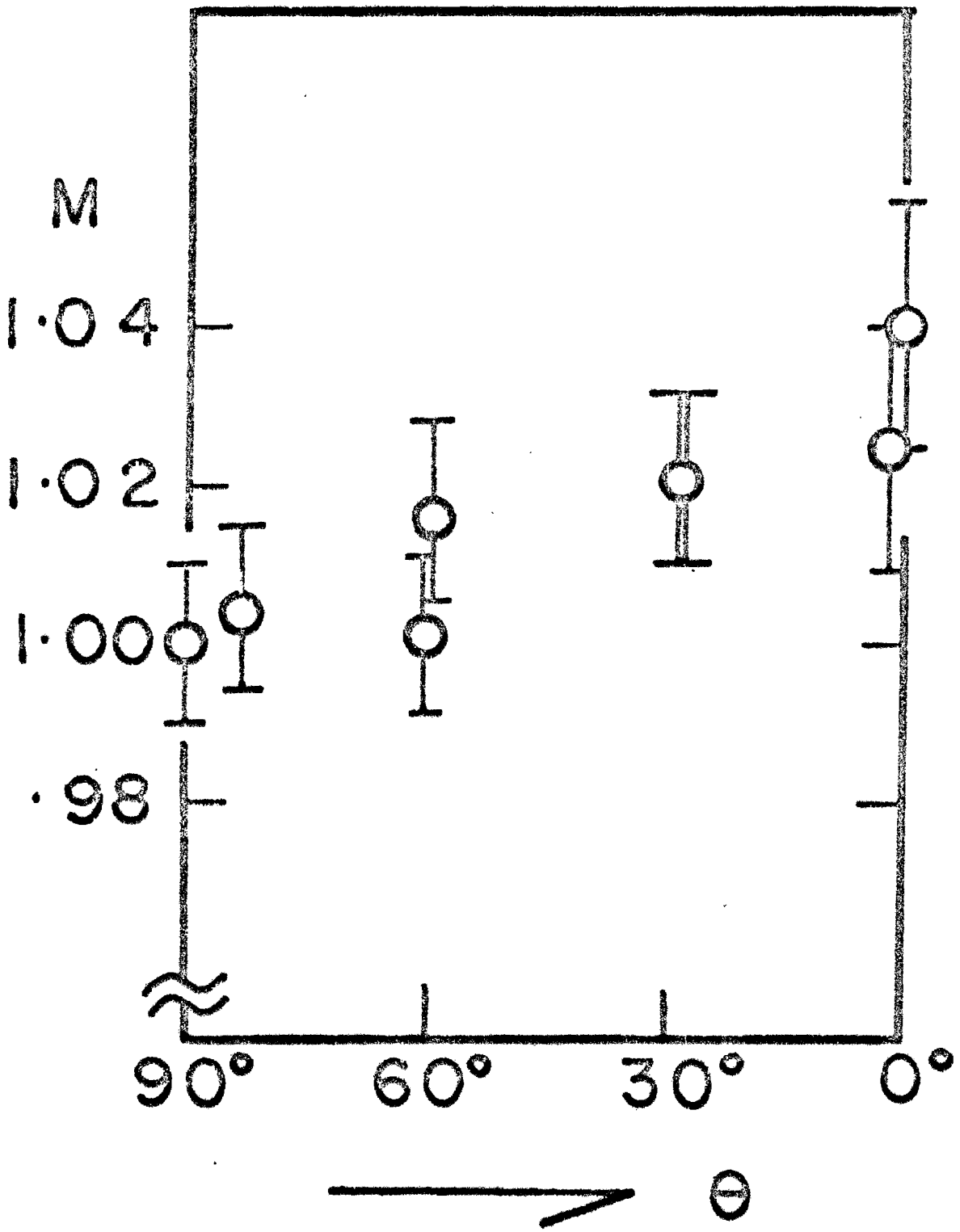

Fig. 17

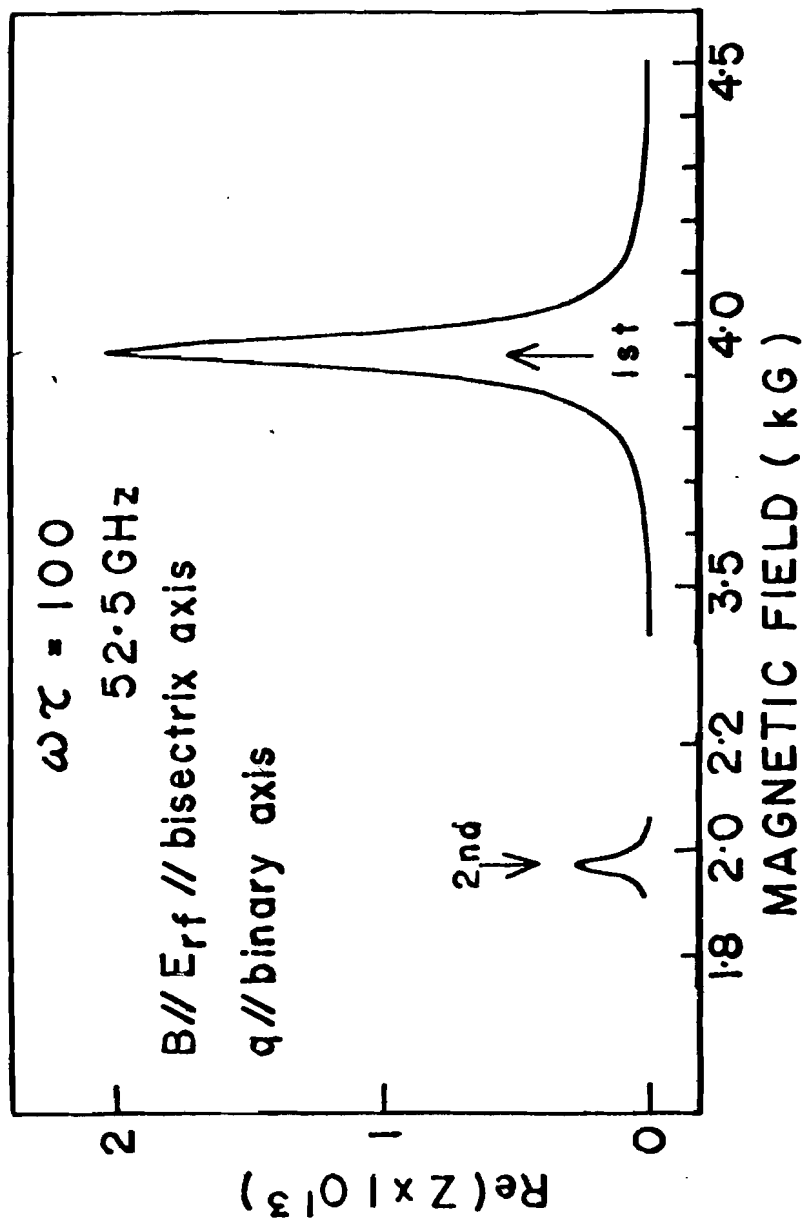
ωτ = 100
52·5 GHz
B// E_rf // bisectrix axis
q // binary axis
2nd
1st
Re(Z x 10^3)
0
1
2
1·8
2·0
2·2
3·5
4·0
4·5
MAGNETIC FIELD (kG)

Fig. 18

R (x 10^12)
0.5
100
200
300 GAUSS
he1
e·e·hy
he2
le1
he4
he3
le3 le2
he5

Fig. 19

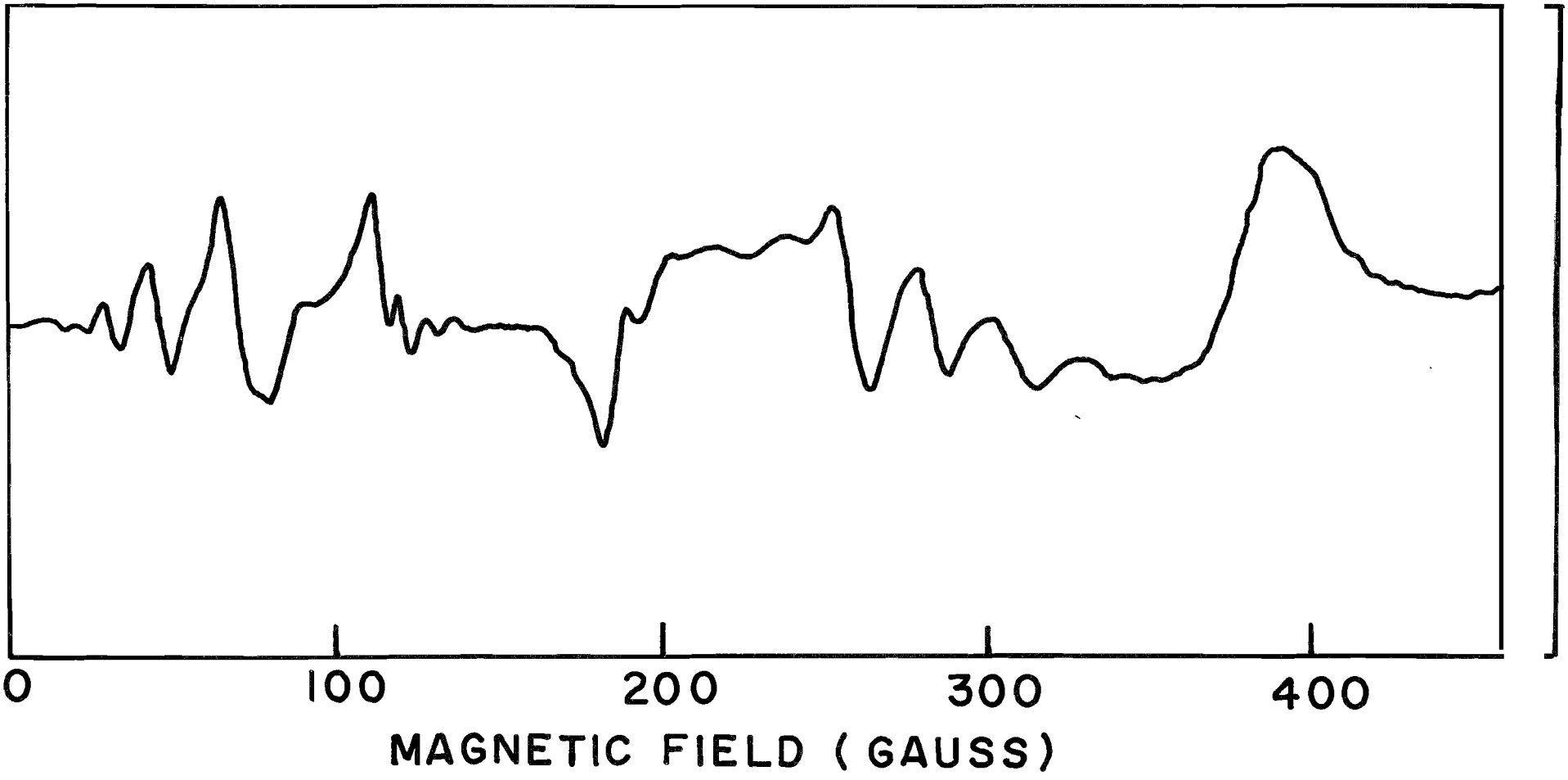

Fig. 20

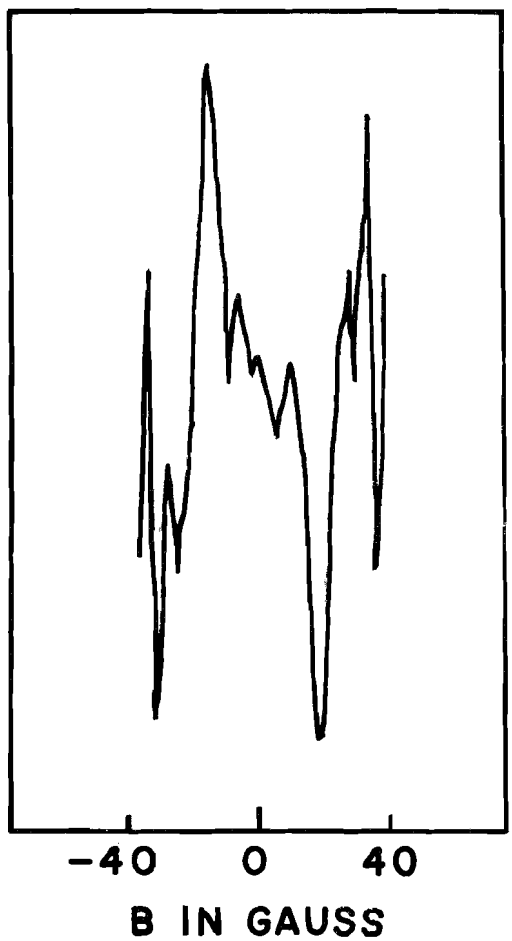

Fig. 21

Figure Captions

Fig.1 For the extraordinary mode, we expand the effective conductivity for fictitous semimetal having spherical electron and hole energy surfaces. We can find the root of the dispersion relation by the cross points of q^2 and ε^* as a function of q. $\varepsilon^* = \varepsilon_{yy} + \varepsilon_{xy}^2/\varepsilon_{xx}$

Fig.2 Plot of the wave number for the coupled mode near the second harmonic of the hole cyclotron resonance as a function of magnetic fields for the fictitous semimetal.

Fig.3 Microwave absortion from a bismuth single crystal as a function of magnetic field (derivative curve). $\vec{q}$//binary, $\vec{B}$//bisectrix, $\vec{E}_{rf}$//trigonal axis; f=46.94GHz, T=1.6°K, d=2.035±0.005mm. The peak at 16.75KG is the electron spin resonance of DPPH, the peak at 1.79KG is "the second harmonic cyclotron resonance" (longitudinal excitation). The periodic interference with respect to the inverse magnetic field is due to the Alfven waves.

Fig.4 Microwave reflection from a slab of a bismuth single crystal as a function of magnetic field (derivative curve). $\vec{q}$//binary, $\vec{B}$//bisectrix, $\vec{E}_{rf}$//trigonal axis; f=52.5GHz, T=1.6°K. The sample thickness d is 0.715±0.003mm.

Fig.5 Microwave reflection from a wedge-shaped bismuth single crystal as a function of magnetic field (derivative curve). $\vec{q}$//binary,

$\vec{B}$//bisectrix axis; f=52.0GHz. The sample has a wedge angle of 3 degrees.

Fig.6 Microwave reflection from a slab of a bismuth single crystal as a function of magnetic field (derivative curve). $\vec{q}$//binary, $\vec{E}_{rf}$//$\vec{B}$//bisectrix axis, f=52.5GHz, d=0.411±0.002mm.

Fig.7 Microwave reflection from a wedge-shaped bismuth single crystal as a function of magnetic field (derivative curve). $\vec{q}$//binary axis, θ =27°, f=52.0GHz, where θ is the angle between bisectrix axis and magnetic field (yz-plane).

Fig.8 Microwave reflection from a bismuth single crystal as a function of magnetic field (derivative curve). $\vec{q}$//trigonal, $\vec{B}$//bisectrix, $\vec{E}_{rf}$//binary axis; f=52.5GHz, T=1.6°K, d=2mm. The arrows A and B correspond to the arrows A and B in Fig. 2 and in Fig. 11.

Fig.9 Dispersion relation of electromagnetic waves for 46.94GHz as a function of magnetic fields. Open circles are the experimental points obtained from interference patterns. Solid line is a calculated dispersion relation.

Fig.10 Dispersion relation of electromagnetic waves for f=52.5GHz in the vicinity of the second harmonic (1970 Gauss) and the fundamental (3940 Gauss) of the hole cyclotron resonances. The solid lines are the calculated curves for the electromagnetic waves for $\omega\tau$=100 coupled with longitudinal excitations (nonlocal Alfven waves), and the broken lines

are the calculated curves for Alfven waves in the local regime and the longitudinal excitation ω_- (nonlocal) for $\omega\tau = 100$. Dots are the experimental points obtained from interference patterns.

Fig.12 Microwave reflection from a slab of a bismuth single crystal as a function of magnetic field (derivative curve). $\vec{q}$//binary, $\vec{B}$//bisectrix, $\vec{E}_{rf}$//trigonal axis,and f=50.3GHz.

Fig.13 Microwave reflection from a slab of a bismuth single crystal as a function of magnetic field (derivative curve). $\vec{q}$//binary, $\vec{B}$//$\vec{E}_{rf}$//bisectrix axis and f=50.3GHz.

Fig.14 Real part of the surface impedance of magnetic field derivative as a function of magnetic field. The solid line represents the experimental curve for the microwave reflection in the vicinity of the second harmonic of the hole cyclotron resonance. The dotted line is the calculated line shape assuming $\omega\tau$ = 100 and retaining terms up to the order of X^2. The calculated curve was not significantly altered even if higher order terms were retained as shown in Fig. 15.

Fig.15 Real part of surface impedance (calculated) as a function of magnetic field for $\vec{q}$//binary, $\vec{B}$//bisectrix, $\vec{E}_{rf}$//trigonal axis, f=52.5GHz, $\omega\tau$ = 100. The dotted line is the calculated curve for the real paat of the surface impedance in the long wavelength approximation for $X \leq 4$. The solid line represents the curve obtained by adding the contribution for $X \geq 4$ in the short wavelength approximation to the upper result.

Fig.16 Real part of surface impedance (calculated) as a function of magnetic field, for $\vec{q}$//trigonal, $\vec{B}$//bisectrix, $\vec{E}_{rf}$//binary axis, f=52.5GHz and $\omega\tau$= 100. The solid line is the calculated curve for the real part of the surface impedance obtained by adding the long and the short wavelength approximations. The arrows A ans B correspond to the arrows in Fig. 7 respectively and to A and B in Fig. 2.

Fig.17 Shift of anomalies with the angle θ° between $\vec{E}_{rf}$ and $\vec{B}$ ($\vec{q}$//binary, $\vec{B}$//bisectrix axis). Ordinate M is $H_2(\theta)/H_2(90)$, where $H_2(\theta)$ is the middle point of the anomaly near the second harmomic measured relative to the anomaly in extraordinary configuration.

Fig.18 The real part of the surface impedance in the long wave-length approximation ($qR \leq 2$) as a function of magnetic field near the fundamental and the second harmonic cyclotron resonance of the holes for $\vec{q}$//binary, $\vec{B}$//$\vec{E}_{rf}$//bisectrix axis, f=52.5GHz, $\omega\tau$ = 100.

Fig.19 The real part of the surface impedance as a function of magnetic

field, for $\vec{q}$//binary, $\vec{B}$//bisectrix, $\vec{E}_{rf}$//trgonal axis, f=52.5GHz and $\omega\tau$ = 50. The line shape has structure because in the extraordinary mode there may be two modes which are called high frequency waves.

Fig.20 Microwave reflection from a slab of a bismuth single crystal as a function of magnetic field (derivative curve) $\vec{q}$//binary, $\vec{B}$//$\vec{a}$ (the angle between $\vec{a}$ and bisectrix is 40°), f=50.3GHz and d=0.713mm.

Fig.21 Microwave reflection from a slab of a bismuth single crystal as a function of magnetic fiedd (derivative curve) $\vec{q}$//binary, $\vec{B}$//bisectrix.

References

1) J.K.Galt and S.J.Buchsbaum, Phys.Fluids 4 1514 (1961)

2) M.S.Khaikin, R.T.Mina and V.S.Edel'man, J.Exptl.Theoret.Phys. (U.S.S.R.) 43, 2063 (1962)

3) G.E.Smith, L.C.Hebel and S.J.Buchsbaum, Phys.Rev.1 129,154 (1963)

4) Yi-Han Kao, Phys.Rev., 129 1122 (1963)

5) V.S.Edel'man and M.S.Khaikin, J. Exptl.Theoret.Phys. (U.S.S,R.) 49, 107 (1965)

6) G.E.Everett, Phys.Rev., 128,2564 (1962)

7) L.C.Hebel, E.I.Blount and G.E.Smith, Phys.Rev., 138,A1636 (1965)

8) L.C.Hebel, Phys.Rev., 138,A1641 (1965)

9) G.A.Williams, Phys.Rev., 139,A771 (1965)

10) R.T.Isaacson and G.A.Williams, Phys.Rev.,177,738 (1969)

11) R.T.Isaacson and G.A.Williams, Phys.Rev., 185,682 (1969)

12) S.Takano and H. Kawamura, J.Phys. Soc. Jppan, 28,349 (1970)

13) S.Nagata and H.Kawamura, J.Phys. Soc. Japan, 24, 480 (1968)

14) G.E.H.Reuter and E.H.Sondheimer, Proc.Roy. Soc. A195,339 (1961)

15) M.Ya.Azbel'and E.A.Kaner, J.Exptl.Theoret.Phys. (U.S.S.R.) 30,811 (1956)
J.Phys.Chem.Solids, 6,133 (1958)

16) R.E.Prange and T.W.Nee, Phys.Rev., 168,779 (1968)

17) T.W.Nee, J.F.Koch and R.E.Prange, Phys.Rev., 174, 758 (1968)

18) J.F.Koch and J.D.Jensen, Phys.Rev., 184,643 (1969)

19) M.S.Khaikin, J.Exptl.Theoret.Phys., 55,1696 (1968)

20) V.F.Gantmakher, J.Exptl.Theoret.Phys., 42,1416 (1962)
44,811 (1963)

21) R.G.Chambers, Proc.Phys.Soc. (London) 86,305 (1965)

22) T.W.Moore, Phys.Pev., 165,864 (1968).

23) R.G.Chambers, Proc.Phys.Soc. (London) A65,458 (1952)
A238,344 (1957)

24) D.C.Mattis and G.Dresselhaus, Phys.Rev., 111,403 (1958)

25) P.S.Zyryanov, Soviet Phys. J.E.T.P. 13, 751 and 953 (1961)

26) P.S.Zyryanov and V.S.Kalashnikov, Soviet Phys. J.E.T.P.
14,799 (1962)

27) J.J.Quinn and S.Rodriguez, Phys.Rev., 128,2487 (1962)

28) M.H.Cohen, M.J.Harrison and W.A.Harrison, Phys.Rev., 117,937
(1960)

29) S.J.Buchsbaum, Plasma Effects in Solids (7th International
Conference on the Physics of Semiconductors),
3 (1964)

30) I.B.Bernstein, Phys.Rev., 109,10 (1958)

31) C.K.N.Patel and R.F.Slusher, Phys.Rev.Letters 21,1593 (1968)

32) P.M.Platzman, W.M.Walsh Jr. and E-NiFoo, Phys.Rev.,172,689
(1969)

33) P.W.Anderson, Phys.Rev., 100,749 (1955)

34) H.D.Drew and U.Strom, Phys.Rev.Letters 25,1755 (1970)

35) D.Shoenberg, Proc.Roy.Soc., A170,341 (1939)

36) W.J.McG.Tegart, The Electric and Chemical Polishing of Metals

37) I.Yokota, J.Phys.Soc. Japan, 21,1851 (1966)

38) C.Guthmann, J.P.d'Haenens and A.Libchaber (to be published)

39) Kip, Langenberg and Moore, Phys.Rev., 124,359 (1961)

40) W.Buckel, Z. Physik, 154,474 (1959)

41) A.B.Pippard, The Physics of Metals, 1 Electrons, edited by J.M.Ziman (Cambridge Univ. Press 1969) P113

42) R.Kubo, J.Phys.Soc.Japan, 19,2127 (1964)

43) T.Moriya, K.Ohtaka and S.Yanagawa, Phys.Letters, 33A,450 (1970)

44) S.Rodriguez, Phys.Rev.,112,1616 (1958)

45) G.E.Smith, G.A.Baraff and T.M.Rowell, Phys.Rev., 135,A1118 (1964)

46) K.Toyoda and Y.Sawada, (to be published)

47) B.Lax, K.J.Button, H.J.Zeiger and M.Roth, Phys.Rev., 102, 715 (1956)